C2SMART ER

CONNECTED COMMUNITIES WITH SMART MOBILITY TO EQUITABLY REDUCE CONGESTION

A USDOT University Transportation Center

New York University

Rutgers University

University of Washington

Texas Southern University

The University of Texas at El Paso

CUNY- City Tech

North Carolina A&T

Multimodal MultiScale Urban Traffic Control in Connected and Automated Cities

USDOT Award No. 69A3551747124

January 2025

TECHNICAL REPORT DOCUMENTATION PAGE

1. Report No.	2. Government Accession No.	3. Recipient's Catalog No.	
4.Report title Multimodal MultiScale Urban Traffic Control in Connected and Automated Cities		5. Report Date January 2025	
		6. Performing Organization Code:	
7.Author(s) Jeff Ban, Angela Kitali, Shakiba Naderian		8. Performing Organization Report No.	
9. Performing Organization Name and Address Connected Cities for Smart Mobility towards Accessible and Resilient Transportation for Equitably Reducing Congestion Center (C2SMARTER), 6 Metrotech Center, 4th Floor, NYU Tandon School of Engineering, Brooklyn, NY, 11201, United States		10. Work Unit No.	
		11. Contract or Grant No. 69A3552348326	
12. Sponsoring Agency Name and Address Office of Research, Development, and Technology Federal Highway Administration 6300 Georgetown Pike McLean, VA 22101-2296		13.Type of Report and Period Final report	
		14. Sponsoring Agency Code	
15. Supplementary Notes			
16.Abstract This project develops and tests the multiscale, multimodal signal-vehicle coupled control (M^2SVCC) framework to jointly optimize traffic signal control and surrounding vehicles and other road users at urban intersections. Connected and automated vehicles and human-driven vehicles, with diverse energy types, are integrated, together with active road users (pedestrians and cyclists). The proposed M^2SVCC model is tested through both simulation and real-world field test using the Mcity remote access testing facilities (Mcity 2.0). Testing results show that M^2SVCC demonstrates superior performance compared to traditional signal control methods, significantly reducing delays, energy use, and conflicts across various scenarios. Future research will focus on integrating learning-based approaches and scaling the model to larger, more complex networks to further enhance multimodal urban transportation management.			
17. Key Words Multimodal traffic Control, Signal-Vehicle Coupled Control (SVCC), Connected and Automated Vehicles (CAVs), Active Transportation Users, Pedestrian and Cyclists		18. Distribution Statement No restrictions. This document is available to the public through the National Technical Information Service, Springfield, VA 22161. http://www.ntis.gov	
19. Security Classif. (of this report) Unclassified	20. Security Classif. (of this page) Unclassified	21. No. of Pages	22. Price

Form DOT F 1700.7 (8-72) Reproduction of completed page author

Multimodal MultiScale Urban Traffic Control in Connected and Automated Cities

Principal Investigator
Xuegang (Jeff) Ban
University of Washington
0000-0003-3605-971X

Co PI
Angela Kitali
University of Washington
0000-0002-1962-162X

Student
Shakiba Naderian
University of Washington

C2SMARTER Center is a USDOT Tier 1 University Transportation Center taking on some of today's most pressing urban mobility challenges. Some of the areas C2SMARTER focuses on include:

Developing new technologies, operational policies, and strategies towards ensuring system-level congestion reduction for all users.

Building on top of the foundational creation, calibration, and validation of our unique network of testbeds, both physical and cyber, to validate and synthesize insights across cities, and focus on transitioning research into practice for positive, equitable, impacts.

Following the principles of the USDOT strategic goal of transformation, using evidence-based decision making to turn research into transformative and equitable solutions that take advantage of emerging technologies.

Led by the New York University Tandon School of Engineering, C2SMARTER's geographically diverse consortium includes: Rutgers University, University of Washington, the University of Texas at El Paso, CUNY- City Tech, Texas Southern University, and North Carolina A&T.

Visit c2smarter.engineering.nyu.edu to learn more.

Disclaimer

The contents of this report reflect the views of the authors, who are responsible for the facts and the accuracy of the information presented herein. This document is disseminated in the interest of information exchange. The report is funded, partially or entirely, by a grant from the U.S. Department of Transportation's University Transportation Centers Program. However, the U.S. Government assumes no liability for the contents or use thereof.

The findings and conclusions in this report have not been formally peer reviewed. Any aspect of the research may change as a result of future research or review.

Acknowledgements

In addition to the funding support from C2SMARTER, the field testing of the proposed M^2SVCC algorithm was jointly conducted on the Mcity 2.0 CAV testbed at the University of Michigan. The support from the faculty, researchers, and graduate students from Mcity is greatly appreciated.

Executive Summary

New advancements enabled by connected and automated vehicles (CAVs) have made possible effective cooperation between road users and traffic infrastructure toward more efficient and safer mobility. This study aims to advance a Signal-Vehicle Coupled Control (SVCC) model to jointly optimize traffic and vehicle control at urban traffic intersections for various transportation modes, including active transportation and vehicles with different types of energy consumption (e.g., fuel, hybrid, and electric). The study also conducts a field-test of the SVCC model on the Mcity 2.0 testbed in Ann Arbor, Michigan, to evaluate the performance of the model in real-world scenarios.

In this project, we aim to expand the unimodal SVCC to a multiscale, multimodal SVCC (M2SVCC) to explore and study the balances when incorporating active transportation and other multimodal considerations. Initial results from integrating pedestrians and cyclists into the optimization process show that M2SVCC outperforms traditional methods, such as actuated signal timing plans, in reducing delays and conflicts. The model demonstrated improvements in performance across various pedestrian phasing settings, including both concurrent and exclusive settings. While the exclusive phasing scheme prioritizes safety, the concurrent phasing leads to more significant improvements in mobility. This highlights how different settings may help balance mobility and safety, depending on the desired policy objectives.

Future work should focus on exploring learning methods, such as Imitation Learning, knowledge distillation, and Deep Reinforcement Learning, to enhance the management of multimodal signalized intersections with CAVs. Additionally, more numerical results and analyses should be provided to demonstrate the effectiveness of the M2SVCC framework, particularly in larger networks with multiple intersections. Finally, the implementation and testing of the M2SVCC framework, including the integration of pedestrians and cyclists, should be tested in real-world and/or CAV testbeds such as the Mcity 2.0 testbed.

Table of Contents

List of Figures

List of Tables

1. Introduction

1.1. Project Background

Urban transportation systems are characterized by the diverse and interactive dynamics of various travel modes, including vehicles of various types and active transportation users such as pedestrians and bicyclists. From the perspective of urban traffic management and control, urban traffic is also multiscale in both time and space: from fast operation/control of vehicles (and individual users) to intersection-level management and control, corridor and sub-network local control, and network-level global control (Guo and Ban, 2023), with increasingly larger temporal and spatial scales. Despite the inherently multimodal, multiscale nature of traffic in modern cities, most existing studies tend to focus on the mobility of a single mode and/or a single scale of traffic, often neglecting the need for a comprehensive and unified perspective that integrates different modes and scales altogether.

Recent advancements enabled by connected and automated vehicles (CAVs) in the field of Intelligent Transportation Systems (ITS) has provided promising solutions to many transportation challenges (Guo et al., 2019; Shladover, 2018). These technologies offer enhancements in urban traffic control (UTC) by enabling cooperative interactions between vehicles and active users with the surrounding environment and providing greater control flexibility through automation. The connected, cooperative, and automated capabilities of these new technologies facilitate the coordination of mobility between different road users and traffic infrastructure (Piperigkos et al., 2022). CAVs also enable advanced control strategies to improve eco-driving, reduce delays, and enhance safety (Han et al., 2020; Sun et al., 2020; Yao & Li, 2020; Yu et al., 2018). For a comprehensive review, see Guo et al. (2019).

The interdependent and multiscale interactions between traffic control and vehicle movements—where vehicles follow signal plans operating on different time scales, and signals are dynamically updated based on traffic flow—have driven the development of multiscale Signal-Vehicle Coupled Control (SVCC) modeling framework (Guo & Ban, 2023, 2024). SVCC aims to simultaneously optimize vehicle trajectories and signal timings, minimizing overall intersection delays and vehicle fuel consumption. Despite extensive research on signal planning and optimization in CAV environments, significant gaps remain in addressing multimodal control challenges. Most studies focus on vehicular traffic, overlooking the interactions among pedestrians, cyclists, and vehicles with varying power systems (gasoline, hybrid, electric, etc.). This illustrates the need for comprehensive, multi-objective approaches to urban traffic management that reflect real-world multimodal traffic dynamics. Moreover, despite abundant research developed on CAV control schemes at intersections including the multiscale SVCC methods, most are tested in virtual simulation-based scenarios (McConky & Rungta, 2019; Pourmehrab et al., 2020; Yu et

al., 2018; Guo and Ban, 2023, 2024), while real-world applications of such traffic control strategies with CAVs are sparse (Ban et al., 2020). To address this gap, CAV related field testing is essential for ensuring their safety and reliability, especially in light of recent accidents involving autonomous vehicles (*AV Crashes*, 2024; Lee et al., 2024)

Incorporating active transportation into the multiscale SVCC model is essential for more inclusive and sustainable transportation systems. Active modes of travel, such as walking and cycling, play a critical role in reducing traffic congestion and noise, improving public health, and decreasing carbon emissions (Brand et al., 2021; Mueller et al., 2015; Rabl & de Nazelle, 2012; Sallis et al., 2004). However, these modes often operate on different time scales and spatial dynamics compared to motorized vehicles. Their behavior is also harder to predict and cannot be directly controlled like CAVs, making their inclusion in traffic signal optimization a complex but necessary challenge. Few studies have integrated non-vehicular road users into CAV intersection optimization. Niels et al. (2020a) proposed adding a demand-responsive signal for pedestrians and bicyclists (Niels et al., 2020b) into a signal-free intersection with CAVs, while later work integrated pedestrian signal timing into CAV trajectory optimization (Niels et al., 2024). Other studies explored the use of automated pedestrian shuttles to address pedestrian mobility challenges in CAV-dominated intersections (Jiang et al., 2024; W. Wu et al., 2022), though such solutions may not be considered multimodal as they suggest removing interactions between pedestrians and CAVs by transporting pedestrians in shuttles and thus creating an all-CAV environment.

CAVs also make it possible to incorporate the different features of diverse vehicle types, including electric and hybrid, in addition to traditional fuel-powered vehicles (IEA, 2024), such that their distinct emission profiles and operational characteristics can be accurately captured to create eco-friendly strategies in signal timing optimizations (Khalighi & Christofa, 2015; Osorio & Nanduri, 2015).

Unlike simulated environments, real-world conditions introduce unpredictable variables such as fluctuating weather, diverse traffic scenarios, and varying road conditions that can significantly impact CAV performance. Evaluating SVCC schemes in field tests is vital for bridging the gap to real-world applications. It allows for the validation and fine-tuning of the control algorithms, ensuring their robustness and resilience under real-world conditions. Through field testing, developers can identify issues not apparent in simulation environments, ultimately enhancing the safety, efficiency, and public trust in CAV technologies.

Feng et al. (2018) presented one example of field testing for CAVs. In their study, an augmented reality testing environment was presented to evaluate the performance of a CAV in two scenarios of railway crossing and red-light running in the Mcity testbed in Michigan. The proposed system comprises three main components: a simulation platform, testing CAVs, and a communication network. It synchronizes the real-world movements of testing CAVs with simulation, allowing them to interact with virtual

background traffic as if in a real-world traffic environment. Fayazi et al. (2019) used a verification framework for testing their intersection control scheme (Fayazi & Vahidi, 2018) on autonomous vehicles. The framework employs a vehicle-in-the-loop (VIL) environment by integrating a microscopic traffic simulator, a real AV, and an intersection control server. The server uses a mixed-integer linear program (MILP) to optimize signal timing and vehicle trajectories. The testing, however, assumes all the vehicles are CAVs. VIL simulations have also been explored for CAV testing, focusing on intersection performance and cooperative adaptive cruise control (Ma et al., 2018a, 2018b). Using a VIL testing system consisting of a CAV, traffic signal controller, VISSIM simulator, and communication devices, Ma et al. (2018a) tested a queue-aware signalized intersection approach and departure algorithm in a V2I environment. This setup aimed to optimize vehicle speed at a signalized intersection. The signal phases, however, were operated under a fixed-time control method and not dynamically optimized.

1.2. Research Objectives

Our research extends the single-mode (vehicular only) SVCC framework to include multiple transportation modes, focusing on the efficiency and safety of active users, such as pedestrians and cyclists, while also incorporating energy-efficient strategies for diverse vehicle types. We incorporate pedestrians and cyclists into the model using a Model Predictive Control (MPC) scheme. Pedestrians are included in the SVCC optimization problem through a multi-objective optimization algorithm. Two scenarios for pedestrian crossings are considered: (1) concurrent pedestrian signal phases and (2) exclusive pedestrian signal phases. In the concurrent scenario, pedestrian crossings occur concurrently with parallel vehicle phases, whereas in the exclusive scenario, all vehicle movements are stopped during the pedestrian phase, granting exclusive crossing time for pedestrians. Cyclists are also integrated into the model in both separated bike lanes and mixed vehicle-bicycle flow. We try to address the challenges that exist in modeling the interactions between human-driven vehicles (HDVs) and bicycles and automated vehicles by utilizing car-following models and a unified follow-the-leader approach developed for different road users (Zhao & Zhang, 2017). Lastly, an energy consumption optimization objective is formulated to achieve energy-efficient trajectories for all vehicle types such as electric, hybrid, and Internal Combustion Engines (ICEs), accounting for their distinct emission profiles.

Through a collaboration between the project team and Mcity researchers at the University of Michigan (U-M), this research aims to evaluate the performance of the proposed SVCC model and algorithm on controlling the real-world traffic and signal timing plans at signalized intersections in the presence of CAVs under both 100% penetration and mixed-flow scenarios. We mainly plan to answer three questions: (1) What is the performance of the SVCC algorithms in a real-world traffic environment (i.e., Mcity test facility)? (2) How to evaluate the performance of the SVCC algorithm in a mixed traffic environment? and (3) How can we extend the algorithms to a larger urban environment? By answering these questions, we hope to bridge the gap between simulation-based studies and real-world applications, demonstrating that the SVCC algorithm is effective in real-world situations with various

mixed flow conditions and is adaptable to different traffic conditions due to its versatile features and configuration capabilities. The evaluation takes place through field testing at the Mcity field site, located in the U-M's North Campus in Ann Arbor, Michigan. The field test involves a synchronized interactive environment, called *Mcity 2.0* (Mcity Website, 2024), including a mobility data center, a simulation platform, and real CAVs. The Multiscale SVCC algorithm is tested on the physical infrastructure at Mcity, by remotely controlling CAVs and traffic signals at the University of Washington (UW).

The main contribution of the research is as follows:

- Proposing an SVCC algorithm that accounts for both the multiscale and multimodal nature of UTC.
- Integrating active transportation users and energy-efficient modeling strategies into the system, while exploring the necessary balances and trade-offs to ensure efficient performance for all modes at signalized intersections with CAVs.
- Implementing and evaluating the performance of SVCC on the Mcity 2.0 testbed, illustrating the potential and challenges of SVCC in future connected and automated cities.

1.3. Report Organization

This report will focus on the development of a multimodal, multiscale SVCC (M^2SVCC) framework and its implementation on real-world testbed Mcity 2.0. The remainder of this report is structured as follows: Section 2 will provide a review on unimodal multiscale SVCC, the model that motivates the current study. Section 3 describes the methodology to incorporate different modes (i.e., pedestrians, cyclists, and vehicles with different types of energy consumption). The preliminary simulation-based results of multimodal, multiscale SVCC are presented in Section 4. Section 5 will provide the descriptions and results on testing unimodal SVCC in the Mcity 2.0 testbed. Lastly, Section 6 presents the conclusion and future directions of the study.

2. Review of unimodal multiscale SVCC for vehicular traffic

As shown in Figure 1, UTC contains several scales (levels), from vehicle level, intersection level, corridor level, sub-network level, to the whole network level. Traffic at different scales interact with each other (especially with their neighboring scales), while having their own dynamics (Figure 1). Both spatial and temporal contexts vary by scale. For instance, vehicle control operates in sub-seconds due to safety considerations, whereas intersection control usually runs in seconds or minutes.

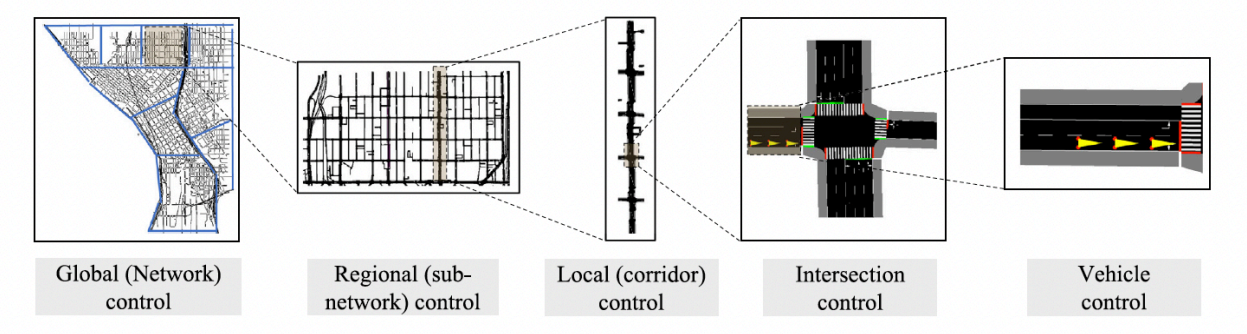

Figure 1. Multiscale nature of urban traffic control (UTC) (Guo & Ban, 2023)

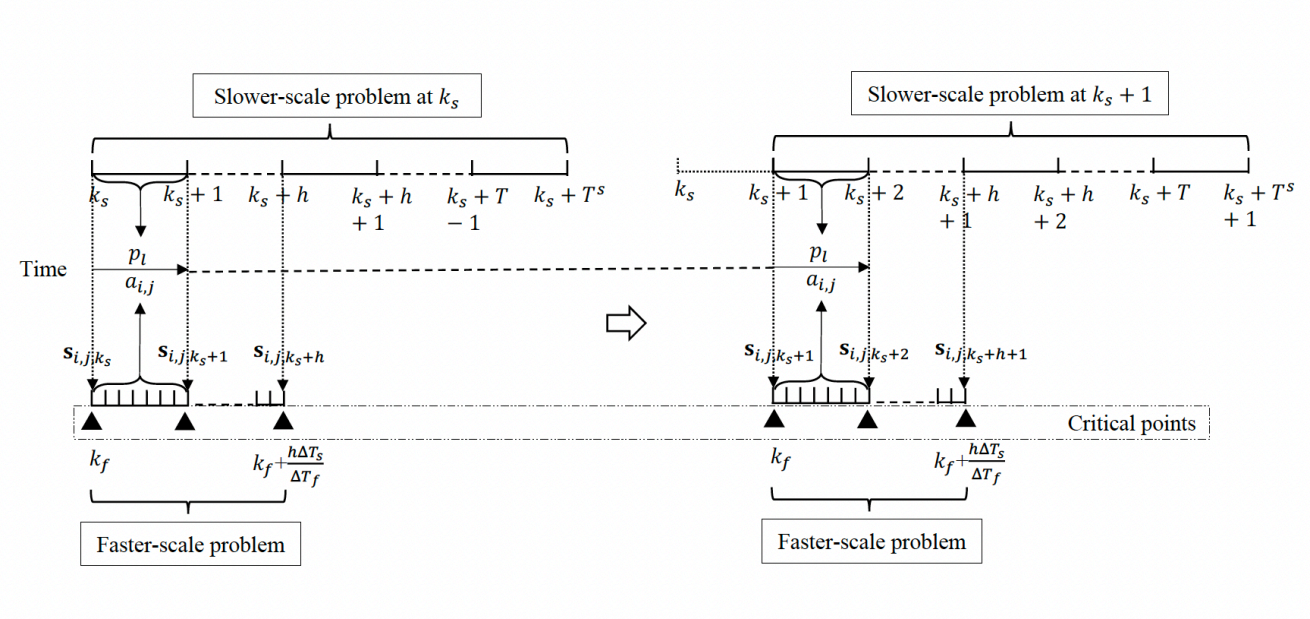

Figure 2. The decomposition and approximation framework (Guo & Ban, 2023)

The Multiscale SVCC model developed by Guo & Ban (2023) aims to optimize both traffic signal timing and vehicle trajectories—including speed, acceleration, and position—simultaneously. It addresses the

challenge of different spatial and temporal scales, as the objectives for intersection control (e.g., minimizing total delay and maximizing intersection throughput) can differ from those for vehicle control (e.g., minimizing fuel consumption and travel time). By decomposing the main problem into a slower-scale optimization problem for intersections and a faster-scale optimization problem for vehicles, the model seeks to minimize the total delay at intersections and reduce fuel consumption of vehicle trajectories at the same time. This decomposition and approximation are achieved through a Model Predictive Control (MPC) scheme that iteratively calculates optimized objectives over a specific prediction horizon. The model aims to optimize conditions at each step, taking into account the future horizon (Figure 2). All the notations in this report are presented in Appendix 1.

Decomposition framework of the main problem is illustrated in Figure 2. Here, T^s is the number of prediction horizon steps in slower time scale. k_s and k_f represent time steps of slower and faster scale problems, respectively, while ΔT_s and ΔT_f denote their respective step durations. The slower-scale problem determines the optimized signal phases ($p_l = 1$ if phase l is green) and the positions of vehicle i on lane j ($s_{i,j}$) at larger (slower) time steps over the prediction horizon. Using these predicted vehicle positions, the faster-scale problem then calculates the optimized speed ($v_{i,j}$), positions ($s_{i,j}$) and acceleration ($a_{i,j}$) of vehicles at smaller (faster) time steps. Consistency between the two problems is maintained by ensuring that the vehicle positions predicted by the slower-scale problem match those in the faster-scale problem at critical points. The formulation of the two problems is as follows.

Signal control: the slower-scale problem (A mixed-integer nonlinear program (MINLP)):

$$\min_{p_l(\hat{k}_s),\, v_{i,j}(\hat{k}_s)} J = \sum_{j=1}^{J} \sum_{i=1}^{n_j} \sum_{\hat{k}_s=K_s}^{T^s+k_s-1} g_{i,j}(\hat{k}_s)\Delta T_s \tag{2-1}$$

Subject to:

$$s_{i,j}(\hat{k}_s) - s_{i,j}(\hat{k}_s - 1) = \frac{v_{i,j}(\hat{k}_s) + v_{i,j}(\hat{k}_s - 1)}{2}\Delta T_s \tag{2-2a}$$

$$s_{i,j}(\hat{k}_s) - s_{i-1,j}(\hat{k}_s) \geq \tau_h v_{i,j}(\hat{k}_s) + d_0 \tag{2-2b}$$

$$-M g_{i,j}(\hat{k}_s) \leq s_{i,j}(\hat{k}_s) - s_{j,max} \leq M(1 - g_{i,j}(\hat{k}_s)) \tag{2-2c}$$

$$g_{i,j}(\hat{k}_s - 1) - g_{i,j}(\hat{k}_s) - r_j(\hat{k}_s) \leq 0 \tag{2-2d}$$

$$A\left[p_1(\hat{k}_s),\, p_2(\hat{k}_s),\, \ldots, p_L(\hat{k}_s)\right]^T = \left[r_1(\hat{k}_s),\, r_2(\hat{k}_s),\, \ldots, r_J(\hat{k}_s)\right]^T \tag{2-2e}$$

$$\sum_{l=1}^{L} p_l(\hat{k}_s) = 1 \tag{2-2f}$$

$$p_l(\hat{k}_s),\ g_{i,j}(\hat{k}_s),\ r_j(\hat{k}_s) \in \{0,1\},\ v_{i,j}(\hat{k}_s) \in [v_{min}, v_{max}] \tag{2-2g}$$

The main objective of the slower-scale problem is to minimize the overall travel time of the vehicles at intersection for the whole prediction horizon (equation 2-1) ($g_{i,j} = 1$ if the vehicle has not yet crossed the intersection and is behind the stop line). Equations (2-2a) and (2-2b) capture vehicle dynamics and car-following constraints respectively, with τ_h representing time headway and d_0 the safety distance parameters. (2-2c) determines the state of $g_{i,j}$ based on the distance of the vehicle from the stop line ($s_{j,max}$). Equation 2-2d specifies that if a vehicle passes the intersection at time step $\hat{k}_s$ the corresponding lane would have the right of way ($r_j(\hat{k}_s) = 1$). Equation 2-2e defines the mapping between the signal phase and the lane right of ways, while 2-2f takes account of signal phase rules.

Vehicle control: the faster-scale problem (A nonlinear program (NLP)):

$$\min_{a_{i,j}(\hat{k}_f)} J = \sum_{i=1}^{n_j} \sum_{i=1}^{h\frac{\Delta T_s}{\Delta T_f}+k_f-1} f_{i,j}(\hat{k}_f)\Delta T_f \tag{2-3}$$

Subject to:

$$v_{i,j}(\hat{k}_f) - v_{i,j}(\hat{k}_f - 1) = a_{i,j}(\hat{k}_s - 1)\Delta T_f \tag{2-4a}$$

$$s_{i,j}(\hat{k}_f) - s_{i,j}(\hat{k}_f - 1) = s_{i,j}(\hat{k}_s - 1)\Delta T_f \tag{2-4b}$$

$$s_{i,j}(\hat{k}_f) - s_{i-1,j}(\hat{k}_f) \geq \tau_h v_{i,j}(\hat{k}_f) + d_0 \tag{2-4c}$$

$$s_{i,j}(\boldsymbol{t_{i,j,k_p}}) - s_{i,j,kp} = 0, k_p = 1, 2, \ldots, h \tag{2-4d}$$

$$v_{i,j}(\hat{k}_f) \in [v_{min}, v_{max}], a_{i,j}(\hat{k}_f) \in [a_{min}, a_{max}] \tag{2-4e}$$

The faster-scale problem, on the other hand, aims to minimize the total fuel consumption of vehicles across all approaching lanes over a specified number of critical points (h) (equation 2-3). Equations 2-4a to 2-4c address vehicle dynamics and car following constraints, while equation 2-4d guarantees the consistency between the slower and faster-scale problems. For the stability analysis of the proposed MOC scheme and further details, refer to Guo & Ban (2023). The results from these two problems ultimately provide optimized signal phase timings and vehicle speed commands for the following time step. The function used to calculate the fuel consumption of ICEs in this study is as follows (Vellamattathil Baby et al., 2021):

$$f_{i,j}(k_f) = 0.2736 + 0.05993v_{i,j}(k_f) + 0.3547a_{i,j}(k_f) - 0.005804{v_{i,j}}^2(k_f) + 0.01787v_{i,j}(k_f)a_{i,j}(k_f) + 0.06633{a_{i,j}}^2(k_f) + 0.0001888{v_{i,j}}^3(k_f) + 0.001959{v_{i,j}}^2(k_f)a_{i,j}(k_f) + 0.02447{a_{i,j}}^2(k_f)v_{i,j}(k_f) - 0.04892{a_{i,j}}^3(k_f) \quad (2\text{-}5)$$

The proposed framework is also designed to handle mixed-flow scenarios and network-level optimization of traffic signals and vehicle trajectories (Guo & Ban, 2024). Application of the algorithm to a mixed flow environment consists of three steps:

1- Separating Vehicles: Separating the CAVs from HDVs into their corresponding platoons (Figure 3).
2- Estimating HDV Positions: Estimating the position of each individual HDV using interpolation. While the position, acceleration and speed are known for each CAV and their immediately adjacent HDV (depicted as the blue and black objects in Figure 3), the position of other HDVs are approximated using interpolation methods.
3- Formulating the Slower-Scale Problem: Treating HDVs the same as CAVs. As HDVs may not follow exactly the predicted trajectories, a safety-check procedure is also developed for each CAV to ensure that CAVs follow and interact with HDVs safely (or modify their speeds or positions properly to ensure safe distances with HDVs).

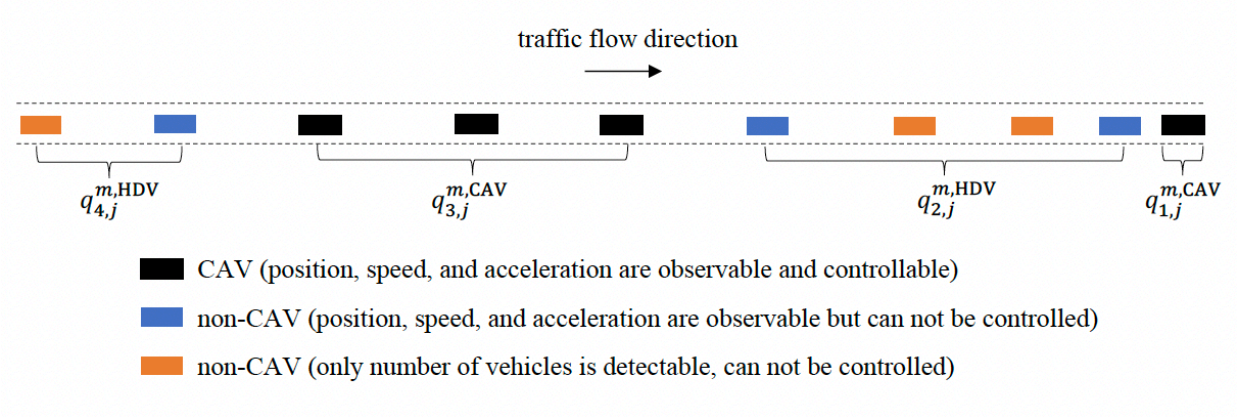

Figure 3. Mixed flow environment at intersection m, lane j (Guo & Ban, 2024)

The Multiscale SVCC model has demonstrated significant improvements over traditional actuated signal control methods, both in single-intersection and network-level settings, across various penetration rate scenarios (Guo & Ban, 2023, 2024). We omit the details here for brevity.

3. Proposed Multimodal, Multiscale SVCC (M2SVCC) Framework

In this section we present the methodology developed for the M^{2}SVCC. This report mainly focuses on the incorporation of active transportation users (i.e., pedestrians and cyclists) and different vehicle types (e.g., ICEs, EVs, etc.). Further studies will focus on the model development for the learning-based methods development for M^{2}SVCC.

In addition to the assumptions of the unimodal SVCC model (i.e., passenger cars only) outlined in Guo & Ban, 2024, the following assumptions are made for M^{2}SVCC studied in this research: It is assumed that the demand for pedestrians and cyclists can be accurately detected using infrastructure technologies such as cameras, detectors, sensors, etc. Also, connected technologies in CAVs enable the communication of critical information, including the energy type of vehicles and other details of surrounding vehicles and other road users approaching the intersection.

3.1. Incorporating Pedestrians into SVCC

To address multimodal objectives, pedestrian delay is explicitly incorporated into the objective function of the slower-scale (intersection-level) optimization problem. The weighted sum of delays for pedestrians and vehicles serves as the objective, while ensuring that phase consistency between pedestrian and corresponding vehicle phases is maintained. Safety considerations are also embedded, such as enforcing the minimum pedestrian green time constraint. The objective aims to optimally derive vehicle trajectories and allocate green phases for both pedestrians and vehicles across all lanes and crossings over the prediction horizon, minimizing the overall delay for all users during this time. The weighting factor in the objective allows balancing priorities between CAVs and pedestrians. Accordingly, the slower-scale objective presented in equation 2-1 becomes:

Multimodal Signal Control (the slower-scale problem):

$$\min_{p_l(\hat{k}_s),\, v_{i,j}(\hat{k}_s)} J = \alpha \sum_{j=1}^{J} \sum_{i=1}^{n_j} \sum_{\hat{k}_s=K_s}^{T^s+k_s-1} g_{i,j}(\hat{k}_s)\Delta T_s + (1-\alpha) \sum_{m} \sum_{k_s} q_m(k_s) D_m(k_s) \Delta T_s \quad \textbf{(3-1)}$$

Subject to (in addition to the 2-2a to 2-2g constraints):

$$B\left[p_l(\hat{k}_s)\right]^T = \left[q_m(\hat{k}_s)\right] \quad \text{(3-1a)}$$

$$\sum_{k_s}^{Gp/\Delta T_s} Pc_l(\hat{k}_s) = 0 \quad (3\text{-}1b)$$

Equations (3-1a) and (3-1b) are added to take account of pedestrian crossing considerations. (3-1a) takes account of mapping between pedestrian and vehicle signal phasing while equation (3-1b) takes account of minimum green time required for pedestrian passing through the intersection. The pedestrian green time (G_p) is calculated based on the following equation (FHWA, 2021). Note that while the inclusion of pedestrian safety constraints as a hard constraint may reduce the flexibility of signal phasing (especially in concurrent pedestrian phases), it ensures safe crossing conditions.

$$G_p = 3.2 + \frac{L}{S_p} + 2.7 * \frac{N_p}{W} \quad (3\text{-}2)$$

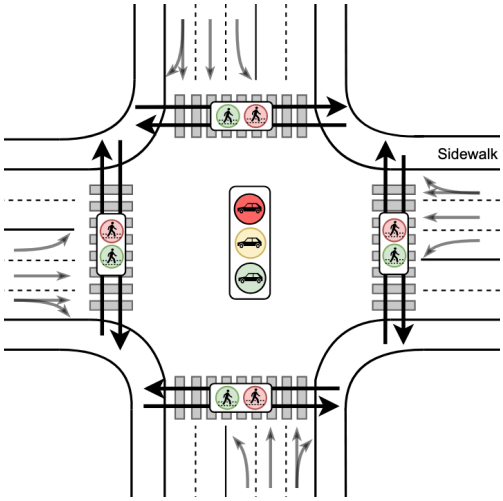

Figure 4. Concurrent pedestrian signal phasing

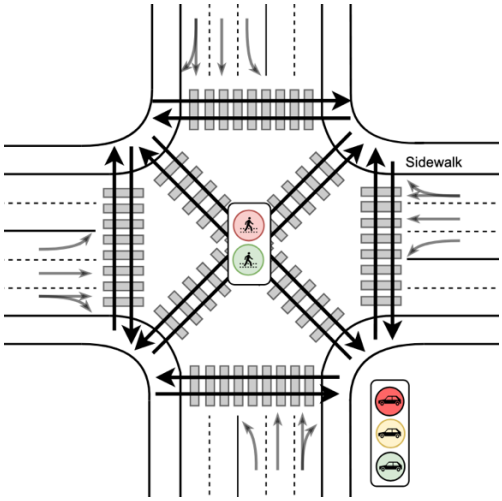

Figure 5. Exclusive pedestrian signal phasing

The proposed model is applied to two scenarios to evaluate its performance under different pedestrian signal phasing strategies: (1) concurrent pedestrian signal phasing (Figure 4), and (2) exclusive pedestrian signal phasing (Figure 5). In the first scenario, pedestrian crossings occur concurrently with parallel vehicle phases. A key constraint here is the minimum pedestrian green time, which ensures pedestrian safety. This safety constraint requires extending the corresponding vehicle signal phases, thereby limiting the flexibility to adjust signal timing solely based on CAV demand. This interaction potentially increases delays for vehicles when pedestrian flows are significant. In the exclusive scenario, on the other hand, all vehicle movements are halted during the pedestrian phase, granting exclusive crossing time for pedestrians. This approach offers greater flexibility for adjusting vehicle signal timings

during the vehicle phases, as pedestrian movements are separated. However, the exclusive pedestrian phase requires a complete stopping of all vehicles from all approaches, which could impact overall traffic efficiency. The objective is to explore how the inherent trade-offs in these scenarios affect system performance in a connected and automated environment, considering both pedestrian safety and CAV traffic demand.

M²SVCC incorporates the signal phases shown in Figure 6 for both concurrent and exclusive pedestrian phasing. Unlike traditional actuated or fixed-time signal timing approaches, M²SVCC operates without a cycle-based signal timing structure. This property enables dynamic adjustments to signal phasing in response to real-time traffic and pedestrian demands.

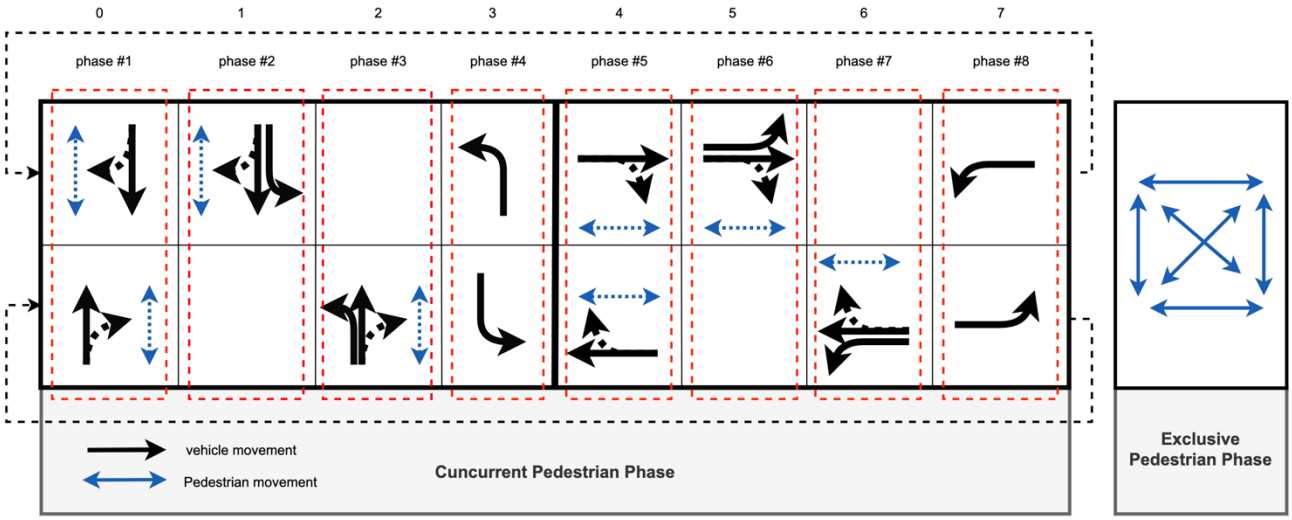

Figure 6. Signal phases in M²SVCC with pedestrians (concurrent and exclusive phasing)

3.2. Incorporating Bicyclists into the SVCC model

Bicyclists are modeled similarly to pedestrians, with a separate signal phase dedicated to bicycles in each approach (Figure 7). The slower-scale objective function is extended to include bicycle delays as follows:

$$\min_{p_l(\hat{k}_s),\, v_{i,j}(\hat{k}_s)} J = \alpha \sum_{j=1}^{J} \sum_{i=1}^{n_j} \sum_{\hat{k}_s=K_s}^{T^S+k_s-1} g_{i,j}(\hat{k}_s)\Delta T_s + \beta \sum_{m} \sum_{k_s} q_m(k_s) D_m(k_s) \Delta T_s + \gamma \sum_{n} \sum_{k_s} q_n(k_s) D_n(k_s) \Delta T_s \quad \textbf{(3-3)}$$

Where $\alpha + \beta + \gamma = 1$. The following constraint is added to the optimization problem.

$$B\left[p_l(\hat{k}_s)\right]^T = \left[r_{j\in B}(\hat{k}_s)\right] \tag{3-3a}$$

The constraint ensures signal phase mapping between the CAV signals and the bike lane signals. It aligns the green phases for bicycles with those of other modes, such as CAVs, to enable smooth and coordinated traffic flow. Note that the initial conditions and assumptions for bicycles (e.g., maximum and minimum speed and accelerations) are also tailored to reflect their unique characteristics compared to passenger cars. Other constraints are excluded here for brevity.

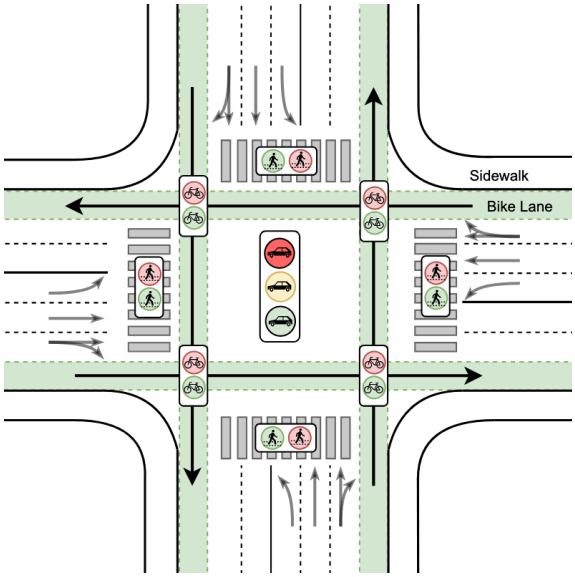

Figure 7. Signalized intersection with pedestrian, bicyclists, and vehicles' signal phasing

M²SVCC accounts for bicycle flows to be present in both separated bike lanes and car lanes (i.e., mixed bicycle-vehicle flow) to achieve a realistic implementation of a multimodal system. Bicycle flows in dedicated bike lanes are treated similarly to HDV flows in vehicle lanes. However, the dynamics of bicycles—such as lower speeds, different acceleration/deceleration profiles, and their interaction with signals—are explicitly modeled to reflect their distinct characteristics. When bicycles share the road with vehicles in mixed-flow conditions, however, we adopt a different approach. In this case, bicycles are treated in a manner similar to HDVs, but their interactions with cars differ from car-to-car interactions. For this reason, we employ the unified follow-the-leader model developed by Zhao & Zhang (2017), to capture the behavior and interactions between bicycles and vehicles in a shared lane. This model provides a more comprehensive framework that allows estimating the states of different modes and their interactions with other modes or boundaries within a shared or dedicated lane. The general form of the equation is as follows (Zhao & Zhang, 2017):

$$m_i \frac{d_{vi}}{d_t} = m_i \frac{v_i^0(t) - v_i(t)}{\tau} + \sum_{j(\neq i)} f_{ij} + \sum_{w} f_{iw} \quad (3\text{-}4)$$

This equation provides the estimation for the product of the object's mass and its acceleration (vehicle or bicycle), which is the net force acting on the object according to Newton's Second Law. The first term on the right-side of the equation represents the object's tendency to move toward a desired speed v_i^0 over a relaxation time period τ. The desired speed is mode-specific and reflects the behavior of the object (bicycle or vehicle). The desired speed for object i is defined based on its distance from an obstacle or leading object d. The equation, derived from experiments with vehicles, pedestrians, and cyclists, is given as:

$$v^0 = \begin{cases} 0 & d < d_{min} \\ k(d - d_{min}) & d_{min} < d < d_{min} + v_{max}/k \\ v_{max} & d > d_{min} + v_{max}/k \end{cases} \quad (3\text{-}5)$$

f_{ij} and f_{iw} are psychological repulsive forces calculated as follows:

$$f_{ij} = A_i e^{(r_{ij} - d_{ij})/B_i} n_{ij} \quad (3\text{-}6)$$

$$f_{iw} = A_i e^{(r_i - d_{iw})/B_i} n_{iw} \quad (3\text{-}7)$$

where f_{ij} represent the interactions between object i and other objects j in its vicinity, and f_{iw} between object i and the boundary of its path (e.g., curb, lane edge) ensures that the object stays within its designated space (i.e., lane). These forces account for the need to avoid collisions and maintain safety. Equations (3-4) through (3-7) are used in this study to capture the state and dynamics of both CAVs and human driven modes (i.e., bicycles and HDVs), providing the state estimation of these modes as inputs for slower-scale and faster-scale optimization models.

3.3. Incorporating vehicles with different energy consumption profiles into SVCC

This study also broadens the scope of vehicle control optimization by addressing energy consumption for various vehicle types, including ICE vehicles, Hybrid Electric Vehicles (HEVs), and Electric Vehicles (EVs). While prior work focused on minimizing fuel consumption for ICE vehicles, the current research adopts a power-based approach to estimate raw energy consumption for HEVs and EVs, bypassing the complexities of their powertrain systems. Inspired by Wu et al. (2015) and Fiori et al. (2016), the total energy consumption, *E*, is computed as (Guo, 2022):

$$E = \int_{t_0}^{t_f} P(t)dt, \tag{3-8}$$

where $P(t)$, the driving power, is defined as:

$$P(t) = \left[ma(t) + mgf_r \cos\theta(t) + mg \sin\theta(t) + \frac{1}{2}\rho A C v^2(t)\right] v(t) \tag{3-9}$$

Here, m represents vehicle mass, $a(t)$ is acceleration, g is gravitational acceleration, f_r is the rolling resistance constant, $\theta(t)$ is the road slope, ρ is air density, A is the frontal area of the vehicle, C is the aerodynamic drag coefficient, and $v(t)$ is the vehicle speed. This comprehensive model captures energy demands due to acceleration, rolling resistance, road grade, and aerodynamic drag, while also accounting for energy regeneration during braking ($P(t) < 0$) for HEVs and EVs.

The objective function for the vehicle control (faster-scale) problem (equation (2-3)) is thus revised to calculate fuel and energy consumption across all vehicle types on an incoming lane *j*:

$$\underset{a_{i,j}(\hat{k}_f)}{Min}\ J = \sum_{i=1}^{n_j} \sum_{\hat{k}_f = k_f}^{h\frac{\Delta T_s}{\Delta T_f} + k_f - 1} P_{i,j}(\hat{k}_f)\Delta T_f \delta_{i,j} + \omega f_{i,j}(\hat{k}_f)\Delta T_f (1 - \delta_{i,j}) \tag{3-10}$$

The objective of the faster problem comprises two main terms, one for EVs and one for ICEs. The first term calculates the total power consumption of EVs over the prediction horizon, while the second term, consistent with Equation (2-3), determines the fuel consumption of ICEs. δ_i is the indicator variable for electric powered vehicles ($\delta_{i,j} = 1$ if the vehicle i on lane *j* is EV or HEV and $\delta_{i,j} = 0$ if vehicle i is an ICE). The parameter ω serves as a weight to convert fuel consumption units into power consumption. We focus on vehicle-level energy consumption in the faster-scale problem because its objective directly considers fuel and power consumption. In contrast, the slower-scale problem operates at the intersection level, aiming to maximize total throughput and minimize overall delay, for which the types of vehicles only have marginal impacts.

4. Simulation results of multimodal multiscale SVCC (M2SVCC*)*

The M^{2}SVCC is tested on a single intersection inspired by one located in Downtown Seattle, Washington (Figure 8). The intersection consists of four approaches, each having three incoming car lanes and one incoming bike lane. At all test cases, two scenarios are compared: (1) actuated signal phasing, and (2) the M^{2}SVCC model. The results of these comparisons are detailed in the following sections. The method and algorithms are implemented in Python and interfaces with the optimization software GAMS, and Simulation of Urban Mobility (SUMO) software via the TraCI package.

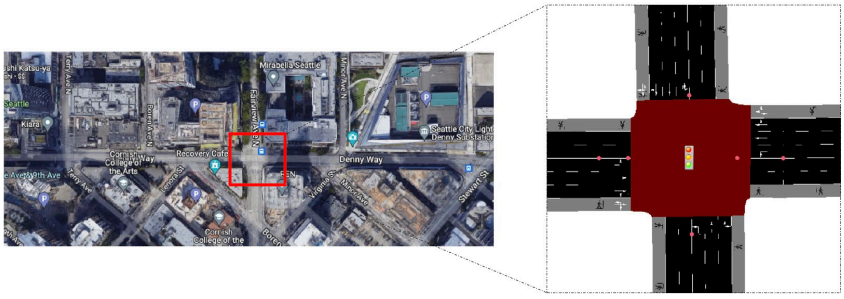

Figure 8. Intersection at Fairview Avenue and Denny Way, Seattle (Guo & Ban, 2023)

4.1. Pedestrians

In the study scenarios (actuated and M^{2}SVCC), we evaluate varying levels of pedestrian demand—low, medium, and high. Additionally, we analyze both symmetric demand distributions, where pedestrian demand is evenly divided across the west, south, east, and north crossings, and asymmetric distributions, where demand is unevenly allocated, with higher concentrations on the west and south crossings compared to the north and east crossings. Scenarios are also analyzed using various weighting factors for pedestrians and vehicles, allowing for flexibility in prioritizing different modes.

In the actuated scenario, traffic signals are controlled based on vehicle demand according to SUMO's default settings. To incorporate pedestrians into the actuated signal scenario for comparability with the M^{2}SVCC framework, the minimum green time for pedestrians (G_p) is applied into the actuated signal phasing scenario. Additionally, the phase is extended using a gap-based extension approach, meaning it continues pedestrian green time signal until a gap in pedestrian demand is observed. This extension occurs even though the actuated signal, influenced by CAVs, indicates a phase change. The extension is stopped, though, if the opposing phase's pedestrians experience excessive delay—specifically, more than 25 seconds. The performance metric used for comparisons are defined as follows:

1- *Average Fuel Consumption (mg/veh/m):* This metric represents the total fuel consumption in milligrams by all vehicles approaching the intersection, divided by the number of vehicles and the average length of the incoming lanes (≈200m).
2- *Average Waiting Time (s/veh):* The total time in which the approaching vehicles' speed was below or equal 0.1 m/s, divided by the number of vehicles.
3- *Average Time Loss (s/veh):* The total time lost due to driving below the ideal speed summed over all the approaching vehicles, divided by the number of vehicles.
4- *Average Queue Length (m):* This metric indicates the average length of the queue from the intersection to the final vehicle in the line.
5- *Average Pedestrian Time Loss (s/ped):* The total time pedestrians spent walking or riding below their ideal speed, divided by the total number of pedestrians.
6- *Number of Conflicts between Pedestrians and CAVs:* The number of instances where pedestrians and CAVs have time to collision (TTC) less than two seconds.

4.1.1. Concurrent pedestrian signal phasing

Signal phases are illustrated in Figure 9, where the four main phases (phases #1, 4, 5, and 8), represented by dashed red lines, are utilized in the actuated scenario. In contrast, four additional phases (phases #2, 3, 6, and 7), bounded by dashed blue lines, are added to M^{2}SVCC to enhance flexibility and improve performance efficiency. The frequency of phase selection by M^{2}SVCC for the asymmetric, medium pedestrian demand scenario is shown in Figure 9. As can be seen, M^{2}SVCC provides greater phase-changing flexibility by allocating more green time to phases 2, 3, 6, and 7—particularly phases 2 and 6, due to the asymmetric pedestrian demand concentrated on the west and south crossings—rather than phases 4 and 8, which only serve vehicular traffic.

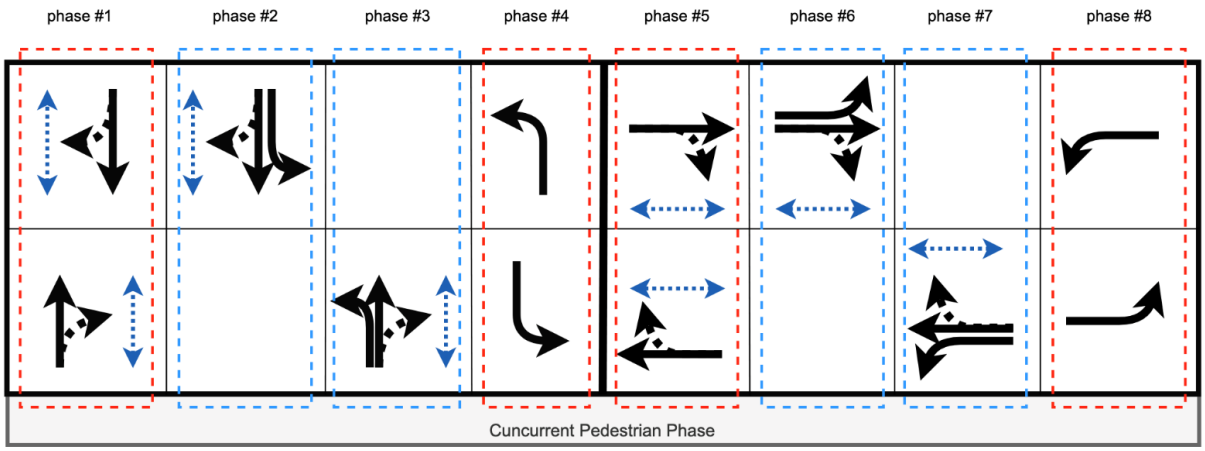

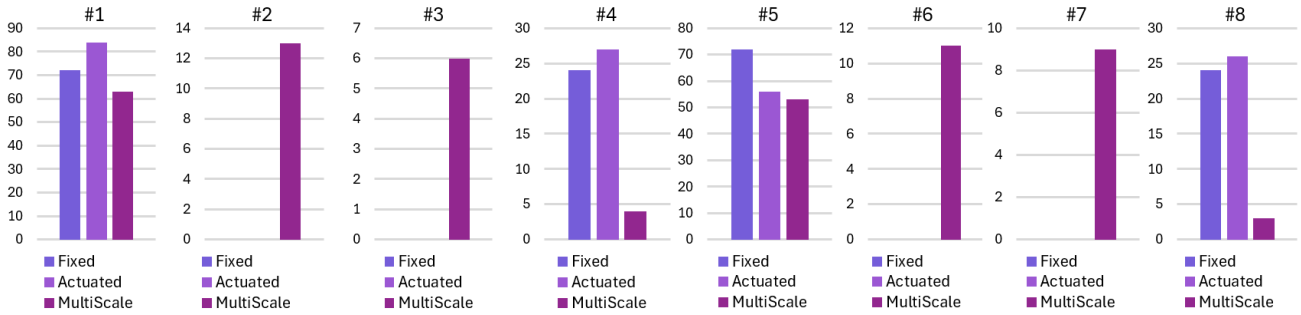

Figure 9. Distribution of phase choices by the fixed, actuated and M²SVCC model with asymmetric, medium pedestrian demand

The performance results across different demand and symmetry scenarios are presented in Table 1 and Table 2. The results include the balanced focus on both modes (50/50 split between vehicles and pedestrians). Other weighting factors are not included, as the results for concurrent phasing are very similar to those of the 50/50 split, which will be discussed in detail later. The percentage change represents the variation of each metric in M2SVCC relative to the actuated control scheme.

Table 1. Performance results for vehicles and pedestrians in symmetric pedestrian demand scenario

Vehicle Demand: 686	**Metrics**	**Actuated**	M²SVCC (vehicle/ped weighting factor) **(50/50)**	M²SVCC (vehicle/ped weighting factor) **% Change**
Low Ped Demand (83)	Fuel Consumption	90.21	56.05	-37.87
	Vehicle Waiting Time	26.03	14.65	-43.72
	Vehicle Time Loss	41.28	29.48	-28.59
	Vehicle queue Length	17.53	11.62	-33.71
	Pedestrian Time Loss	43.78	31.14	-28.87
	# Right-turn conflicts	36	48	33.33
Medium Ped Demand (389)	Fuel Consumption	94.59	60.73	-35.80
	Vehicle Waiting Time	31.84	20.59	-35.33
	Vehicle Time Loss	48.41	37.88	-21.75
	Vehicle queue Length	19.95	13.55	-32.08
	Pedestrian Time Loss	53.16	34.5	-35.10
	# Right-turn conflicts	219	277	26.48
High Ped Demand (822)	Fuel Consumption	96.5	69.72	-27.75
	Vehicle Waiting Time	34.19	34.22	0.09
	Vehicle Time Loss	52.06	54.54	4.76
	Vehicle queue Length	19.49	18.13	-6.98
	Pedestrian Time Loss	55.71	38.63	-30.66
	# Right-turn conflicts	536	706	31.72

Table 2. Performance results for vehicles and pedestrians in asymmetric pedestrian demand scenario

Vehicle Demand: 686	**Metrics**	**Actuated**	M^2SVCC (vehicle/ped weighting factor) **(50/50)**	M^2SVCC (vehicle/ped weighting factor) **% Change**
Low Ped Demand (83)	Fuel Consumption	91.71	55.32	-39.68
	Vehicle Waiting Time	28.19	13.69	-51.44
	Vehicle Time Loss	43.38	28.69	-33.86
	vehicle queue Length	18.53	11.06	-40.31
	Pedestrian Time Loss	41.93	28.33	-32.44
	# Right-turn conflicts	57	58	1.75
Medium Ped Demand (389)	Fuel Consumption	94.58	66.63	-29.55
	Vehicle Waiting Time	32.37	28.91	-10.69
	Vehicle Time Loss	48.85	47.09	-3.60
	vehicle queue Length	19.26	18.16	-5.71
	Pedestrian Time Loss	51.9	34.11	-34.28
	# Right-turn conflicts	226	260	15.04
High Ped Demand (822)	Fuel Consumption	98.64	70.43	-28.60
	Vehicle Waiting Time	36.49	33.79	-7.40
	Vehicle Time Loss	55.19	53.57	-2.94
	vehicle queue Length	21.2	18.38	-13.30
	Pedestrian Time Loss	54.63	40.66	-25.57
	# Right-turn conflicts	553	690	24.77

The results demonstrate that, in nearly all scenarios, M^2SVCC improves the performance of both vehicles and pedestrians compared to the actuated signal timing plan. The only exception occurs when pedestrian demand is high, and the distribution of pedestrian demand is symmetric on the network. In such cases, M^2SVCC fails to show any significant improvements in vehicular time loss and waiting times with respect to an actuated scenario. This is primarily because, in a high-demand, symmetric scenario, where both pedestrian and vehicle flows are heavy (i.e., the intersection is nearly jammed), the order in which signal phases are activated has minimal impact on the overall performance. Since demand is evenly distributed, vehicles and pedestrians experience similar delays regardless of the signal phase sequence, making M2SVCC's adaptive control less effective in reducing time loss and waiting times compared to the actuated control.

It is also evident that M^2SVCC fails to reduce the number of conflicts between pedestrians and right-turning permitted vehicle flow. The lower number of conflicts under fixed and actuated signal scenarios can be attributed to the longer and more frequent activation of phases #4 and #8 in Figure 9. These extended phases provide additional pedestrian clearance time, reducing pedestrian-vehicle interactions,

especially during transitions such as from phase #1 to #4, compared to transitions like from phase #1 to #5. This results in fewer conflicts between pedestrians and vehicles.

It is also observed that in a concurrent phasing scenario, the improvement for vehicles decreases as pedestrian demand increases. However, the benefits of M^{2}SVCC for pedestrian performance, compared to the actuated signal scenario, remain nearly unchanged (Figure 10 and Figure 11).

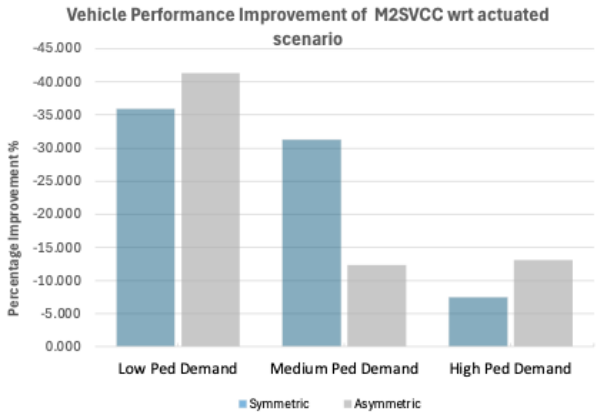

Figure 10. Percentage of improvement of vehicle performance

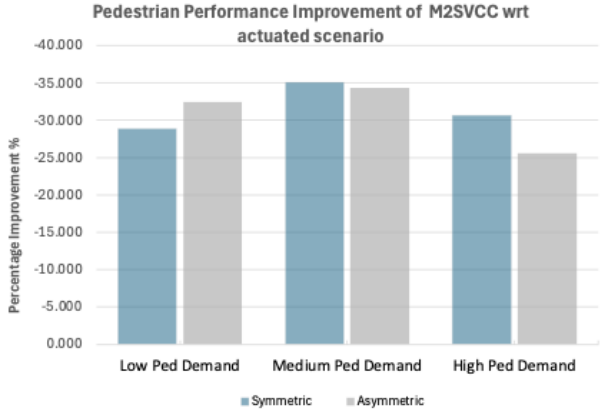

Figure 11. Percentage of improvement of pedestrian performance

4.1.2. Exclusive pedestrian signal phasing

The M^{2}SVCC is also tested on an exclusive pedestrian signal phasing scenario, where pedestrian movements are entirely separated from vehicular traffic through a dedicated signal phase (Figure 5). The exclusive phase significantly reduces conflicts between pedestrians and vehicles compared to the concurrent phasing scenario. This is because right-turning vehicles and pedestrians on parallel crossings no longer interact. The results of vehicle and pedestrian performance in exclusive pedestrian phasing scenario are presented in Table 3.

Table 3. Performance results for vehicles and pedestrians in asymmetric pedestrian demand scenario

Vehicle Demand: 686	Metrics	Actuated	M2SVCC Exclusive Phasing (vehicle/ped weighting factor)						
			0.8/0.2	0.7/0.3	0.6/0.4	0.5/0.5	0.4/0.6	0.3/0.7	0.2/0.8
Low Ped Demand (88)	Fuel Consumption	91.71	54.25	59.39	63.32	66.47	73.19	83.71	107.93
	Vehicle Waiting Time	28.19	10.27	13.38	17.03	21.55	29.09	41.85	71.23
	Vehicle Time Loss	43.38	23.01	27.53	33.07	38.59	48.18	64.05	100.36
	Vehicle queue Length	18.53	8.98	10.17	11.65	13.56	16.11	21.70	34.83
	Pedestrian Time Loss	41.93	82.69	56.46	41.65	41.35	35.74	33.17	30.83
	Right-turn conflicts	57	0	0	0	0	0	1	0
Medium Ped Demand (389)	Fuel Consumption	94.58	60.22	63.82	70.98	78.32	87.21	110.92	158.70
	Vehicle Waiting Time	32.37	14.81	18.78	26.04	34.65	45.88	72.95	126.27
	Vehicle Time Loss	48.85	29.46	34.87	44.47	55.33	68.89	103.62	176.25
	Vehicle queue Length	19.26	11.25	12.55	15.47	18.65	23.34	35.80	60.84
	Pedestrian Time Loss	51.9	58.89	52.61	40.35	38.45	35.27	33.96	29.87
	Right-turn conflicts	226	0	1	4	3	2	1	2
High Ped Demand (822)	Fuel Consumption	98.64	57.89	58.24	63.26	65.61	71.08	80.76	93.96
	Vehicle Waiting Time	36.49	13.92	14.90	19.37	21.75	28.37	39.18	54.85
	Vehicle Time Loss	55.19	28.20	29.14	35.46	38.72	46.66	60.30	80.07
	Vehicle queue Length	21.2	11.66	11.19	12.40	13.59	15.67	20.30	27.77
	Pedestrian Time Loss	54.63	98.21	86.16	58.96	52.55	44.47	41.67	38.02
	Right-turn conflicts	553	1	1	0	2	0	9	12

The results indicate that, across different weighting factors, there are scenarios where both pedestrians and vehicles can benefit significantly from the model. In fact, the exclusive phasing scenario provides greater flexibility in shifting priority between pedestrians and vehicles compared to the concurrent scenario (Figure 12 and Figure 13). By adjusting the weighting factors, a wide range of improvements can be achieved for either mode in the exclusive scenario, allowing intersection control strategies to be adapted based on prevailing policy objectives.

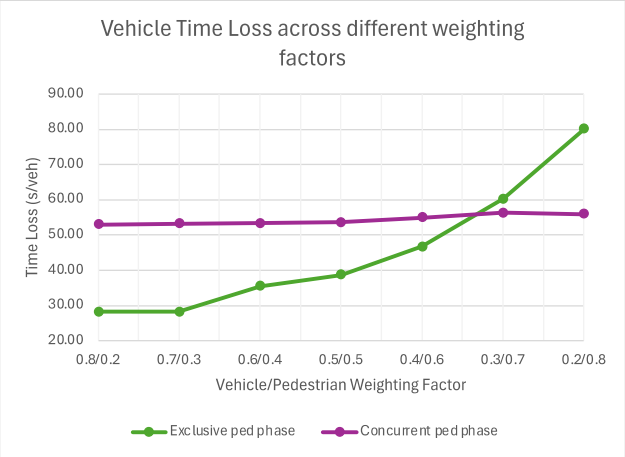

Figure 12. Vehicle time loss across different weighting factors

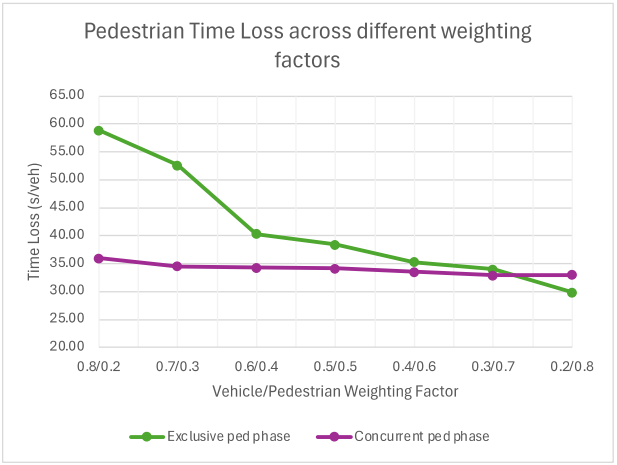

Figure 13. Pedestrian time loss across different weighting factors

To further illustrate this, Figure 14 and Figure 15 present heatmaps showing the percentage improvement in time loss for pedestrians and vehicles under different weighting factors for the high demand scenario. A comparative analysis reveals that M^{2}SVCC effectively adjusts its prioritization based on the assigned importance of each mode in both concurrent and exclusive scenarios. Generally, as the weighting factor for a specific mode increases, the corresponding percentage improvement also rises. However, while improvements remain relatively stable across different weighting factors in the concurrent scenario, the exclusive scenario exhibits significant variations in performance gains or losses. This discrepancy arises because, in the concurrent scenario, the objectives of vehicles and some pedestrians are aligned—pedestrians crossing parallel to vehicle flows benefit from the same green phase. Consequently, adjusting the weighting factors has a limited impact on performance outcomes. In contrast, the exclusive scenario fully separates pedestrian and vehicle movements, making their objectives inherently conflicting. This separation allows for greater flexibility in optimizing each mode's performance using different weighting factors in the weighted sum approach.

When evaluating performance across different settings, two key factors should be considered: mobility efficiency and safety. Regarding mobility efficiency, both concurrent and exclusive settings have shown promising results in improving performance for both vehicles (fuel consumption, waiting time, time loss, and queue length) and pedestrians (time loss). As previously mentioned, in the concurrent setting, adjusting the weighting factors does not significantly impact performance. In contrast, as seen in Table 3 and Figure 12 and Figure 13, the exclusive setting exhibits a specific range of vehicle/pedestrian weighting factors ([0.6/0.4 – 0.4/0.6]) that provide benefits to both modes. To further enhance the safety of active users, assigning pedestrians a slightly higher weight—such as 0.4/0.6—may be a reasonable approach, as vehicle performance still experiences considerable gains under this configuration.

Another key observation is that in the concurrent setting, M^{2}SVCC significantly reduces pedestrian time loss but has a more limited impact on vehicle time loss. This is because, in the concurrent setting, the vehicle phase corresponding to the parallel pedestrian phase must be extended to meet the minimum green time required for pedestrians. Conversely, in the exclusive setting, pedestrian movements are completely halted during vehicle phases, allowing greater flexibility in vehicle phase adjustments without being constrained by pedestrian signal requirements.

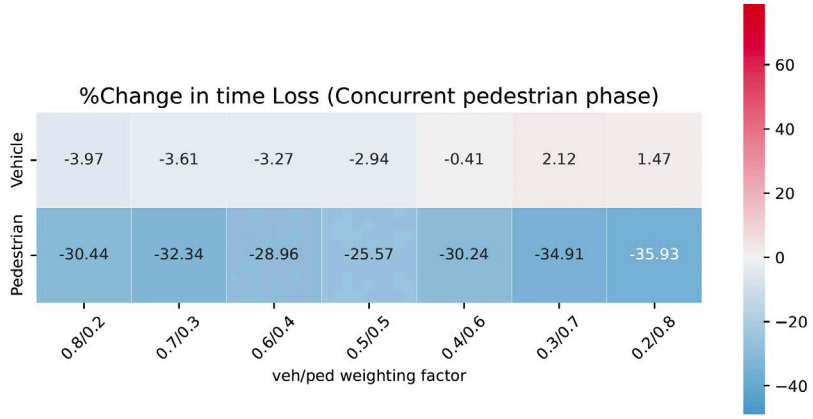

Figure 14. Percentage change in time loss for the concurrent scenario

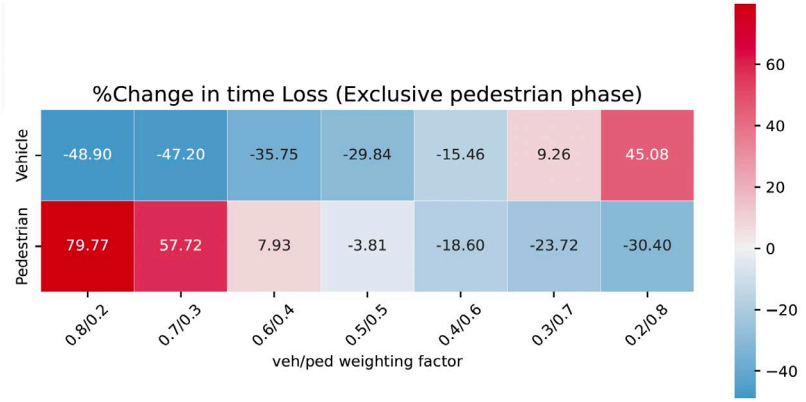

Figure 15. Percentage change in time loss for the exclusive scenario

Lastly, as shown in Table 3, the exclusive pedestrian phasing significantly enhances safety by minimizing conflicts between vehicles and pedestrians. Unlike the concurrent setting (Figure 6), where pedestrian movements occur alongside vehicle phases, the exclusive setting fully separates pedestrian phases, effectively reducing potential interactions and improving overall safety. However, the mobility benefit (such as time loss of pedestrians), as shown in Figure 15, is very moderate under the exclusive pedestrian phasing scheme (especially when compared with the concurrent pedestrian phasing scheme). Therefore, which pedestrian phasing scheme to choose may need to reflect the preferred priority between mobility and safety. If a city prioritizes safety, the exclusive pedestrian phasing scheme may be more desirable.

4.2. Cyclists

The results of integrating cyclists, both on separated lanes and in mixed bicycle-vehicle flows, into the single intersection scenario are presented in Table 4. These results demonstrate that M^{2}SVCC effectively improves the performance of all three modes. The only exception occurs when bicycle and pedestrian demand is particularly high, where M^{2}SVCC does not show improvements in vehicle waiting times or queue lengths. However, the improvements for active transportation modes are consistently significant across various demand scenarios. In this analysis, pedestrians are modeled in a concurrent setting.

Table 4. Performance results for vehicles, cyclists, and pedestrians under asymmetric bike and pedestrian demand

Vehicle Demand: 686	**Metrics**	**Actuated**	Model-based M^{2}SVCC (veh/ped/bike weighting factor) **0.3/0.3/0.3**	Model-based M^{2}SVCC (veh/ped/bike weighting factor) **% Change**
Low Ped (83) and Bike (116) Demand	Fuel Consumption	92.45	61.1	-33.91
	Vehicle Waiting Time	29.63	23.04	-22.24
	Vehicle Time Loss	45.11	37.75	-16.32
	Vehicle queue Length	19.82	16.27	-17.91
	Bike Waiting Time	25.55	16.64	-34.87
	Bike Time Loss	35.28	25.63	-27.35
	Bike queue Length	4.85	3.71	-23.51
	Pedestrian time loss	35.39	28.3	-20.03
Medium Ped (394) and Bike (238) Demand	Fuel Consumption	96.88	68.22	-29.58
	Vehicle Waiting Time	32.55	31.32	-3.78
	Vehicle Time Loss	51.36	48.12	-6.31
	Vehicle queue Length	20.63	18.81	-8.82
	Bike Waiting Time	30.18	16.1	-46.65
	Bike Time Loss	42.2	26.02	-38.34
	Bike queue Length	7.66	5.15	-32.77
	Pedestrian time loss	44.14	32.28	-26.87
High Ped (822) and Bike (490) Demand	Fuel Consumption	115.25	92.052	-20.13
	Vehicle Waiting Time	54.46	62.53	14.82
	Vehicle Time Loss	85.49	85.29	-0.23
	Vehicle queue Length	31.65	32.27	1.96
	Bike Waiting Time	41.12	22.1	-46.25
	Bike Time Loss	57.65	34.97	-39.34
	Bike queue Length	15.49	9.5	-38.67
	Pedestrian time loss	59.1	44.45	-24.79

4.3. Different Vehicle Types

The fuel consumption of ICE vehicles and power consumption of EVs were calculated at the end of the simulation based on equations (2-5) and (3-9), respectively. Figure 16 and Figure 17 show the fuel consumption and power consumption averaged over all ICE vehicles and EVs, respectively, across different EV penetration scenarios. As can be seen, the M^{2}SVCC model successfully improves the fuel and power consumptions with respect to the actuated scenario across different EV penetration rates.

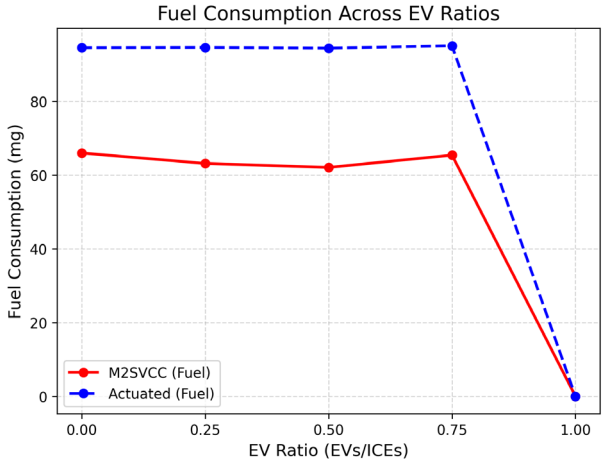

Figure 16. ICE vehicles' average fuel consumption

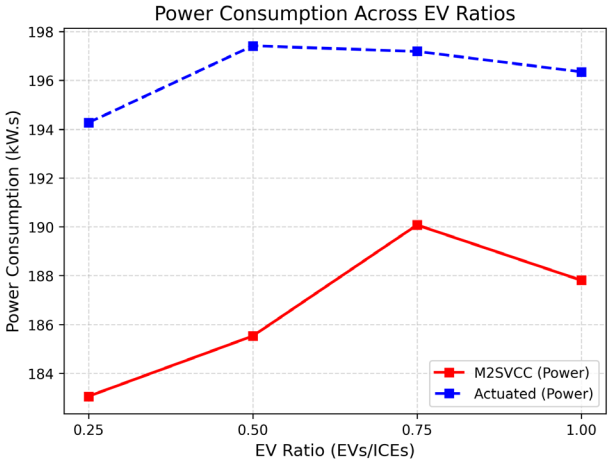

Figure 17. Electric vehicles' average power consumption

5. Testing and evaluation of SVCC in Mcity 2.*0*

The project team collaborated with Mcity researchers on testing the SVCC framework using their newly developed Mcity 2.0 testbed. While the initial attempt was to test and evaluate M^{2}SVCC as presented in this research, due to the extra work to integrate M^{2}SVCC, the remote interface of Mcity 2.0, and needed upgrades to Mcity 2.0 hardware and software systems to facilitate the integration, the team could only finish the field testing and evaluation using Mcity 2.0 for unimodal SVCC for a single intersection, for the duration of this project. The team is currently still working with Mcity researchers to test M^{2}SVCC on a network level, and the results may be presented in subsequent reports or papers.

5.1. Mcity 2.0

Located on a 32-acre site at U-M's North Campus, Mcity features over 16 acres of roads and traffic infrastructure that replicate the complexities of urban and suburban environments. This full-scale outdoor laboratory includes state-of-the-art instrumentation (such as traffic signal control) and sensors, a control network for data collection, mixed-reality testing technology, a fully connected 5G and V2X communication network, and a cloud-based Mcity OS for infrastructure control. The facility offers diverse testing conditions with various road surfaces, traffic signals, and urban features such as a bridge deck, underpass, and a house exterior for first-mile/last-mile testing. Mcity is the world's first full-scale simulated city designed solely for testing the performance of CAVs (Feng et al., 2018; Mcity Website, 2024).

Mcity 2.0 develops digital infrastructure that overlays the physical test facility to enable remote access of Mcity testing facilities through a dedicated application programming interface (API). It provides a cloud-based platform enabling researchers to access Mcity and run test scenarios remotely from any internet-connected device. This cloud-based platform integrates three key components: (1) the Mcity OS, a cloud-based operating system that runs on any internet-enabled device to control all the features of the Mcity test facility and remotely observe and monitor the testing process; (2) TeraSim, a cloud-based traffic environment simulator for testing autonomous vehicles, urban traffic, and traffic control devices. TeraSim creates a detailed virtual model of city traffic with Naturalistic Driving Environment; and (3) the Mcity field-test facilities, the physical infrastructure for mixed-reality vehicle testing.

The connection and communication between these components and the remote researcher are established using the TeraSim APIs (Figure 18). Through the TeraSim API, control commands for CAVs and traffic signals (by UW researchers) are transmitted to TeraSim on the cloud and then sent to the CAVs and traffic signal controller at the Mcity test facility. The background traffic generated through TeraSim is integrated into the testing environment for CAVs, enhancing the capabilities of the test

facility. This mixed reality environment merges a real-world testing facility with a simulation platform, synchronizing the movements of CAVs in the physical world with the simulation. Information about the background traffic is continuously fed to the CAVs, allowing them to interact with virtual traffic as if they were in a real traffic environment (Feng et al., 2018; Feng & Liu, 2019).

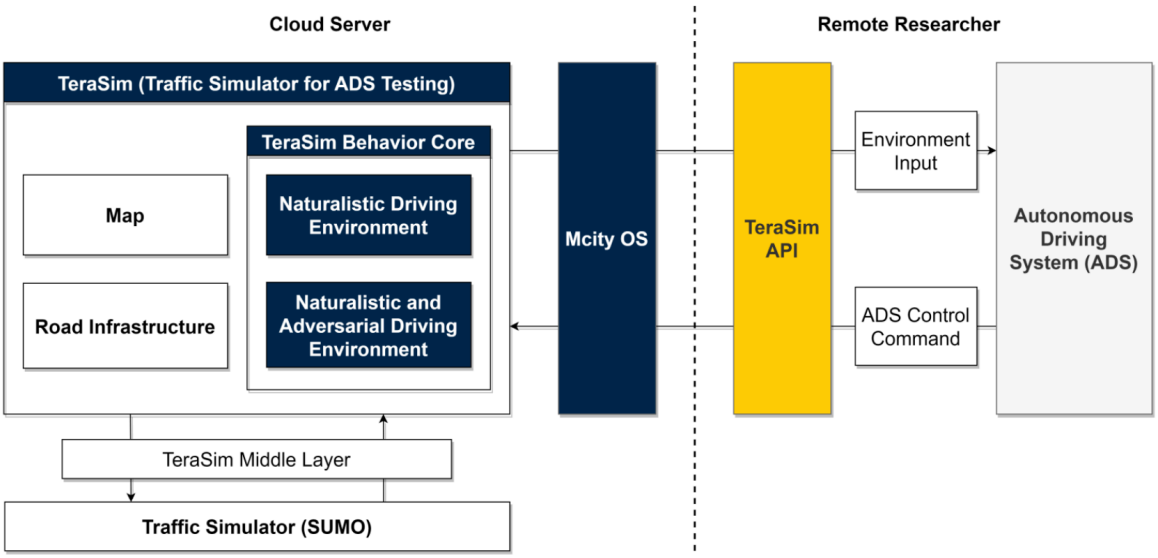

Figure 18. TeraSim API to connect Mcity cloud server and remote researcher (Liu, 2023)

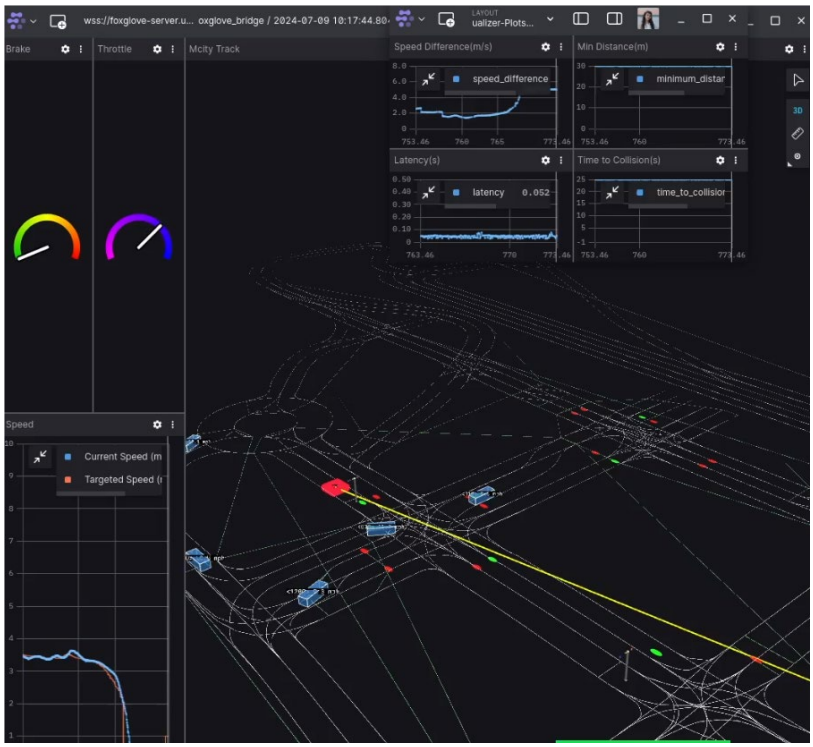

Figure 19. Vehicles, signal status, and ego vehicle's performance metrics (Foxglove visualization tool)

Figure 20. Chasing camera

Figure 21. Onboard camera

All the testing processes can be observed through the Foxglove visualization tool to show vehicles, signal status, and the CAV on the field performance metrics including latency, speed difference, minimum distance, and TTC (Figure 19). Onboard and chasing cameras are also available to observe the actual movements of the CAV in the field test (Figure 20 and Figure 21).

5.2. Integration of SVCC with Mcity 2.0 remote access API

SVCC integration with Mcity facility APIs is presented in Figure 22. Information on current state of the intersection (signal phase, vehicle states, etc.) is collected from the field (or simulation) and sent through TeraSim API to SVCC. Using the MPC algorithm, SVCC calculates the optimized signal phase and vehicle control commands for the current state. Through TeraSim API, these commands are then sent back to the Mcity 2.0 virtual environment (synchronized with the field-test facilities) in order to be applied to the intersection traffic signal and vehicles (CAVs).

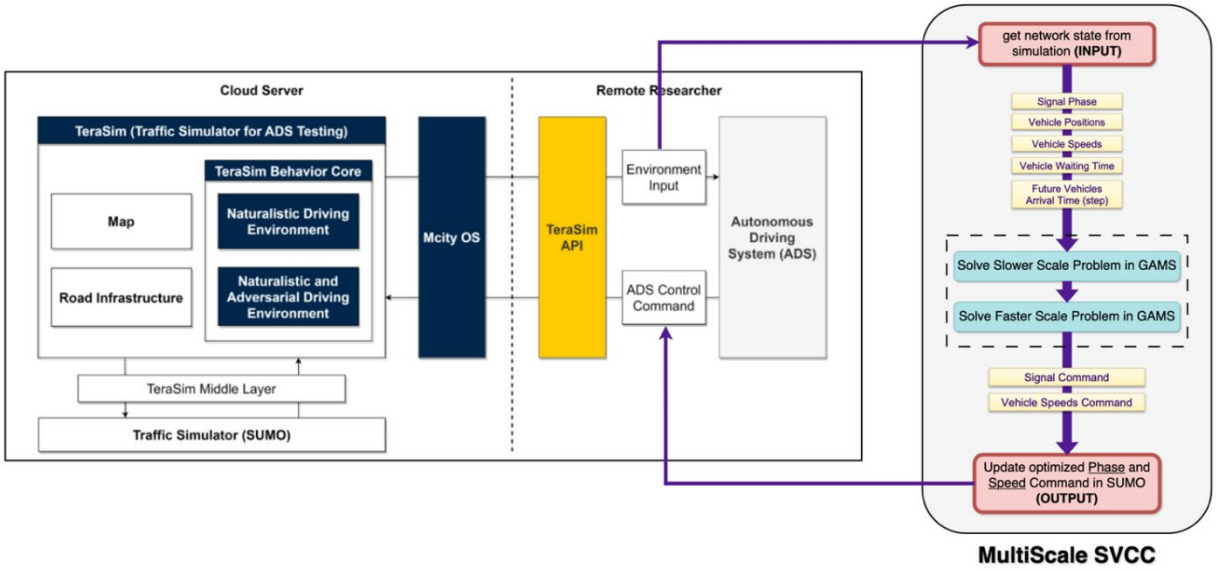

Figure 22. Integration of the SVCC algorithm with Mcity API (Field Testing)

The overview of the whole testing process is also presented in Figure 23. As previously discussed, the information on the intersection status is collected from Mcity digital infrastructure and fed to SVCC using the TeraSim API. After calculating the optimized signal timing and vehicle trajectories, the commands from SVCC are sent back to the Mcity infrastructure to be applied to the vehicles and traffic signals. The testing process can be visually observed through the visualization tools provided by U-M to UW, including onboard and chasing cameras, as well as vehicle and signal status (Figure 19 through Figure 21).

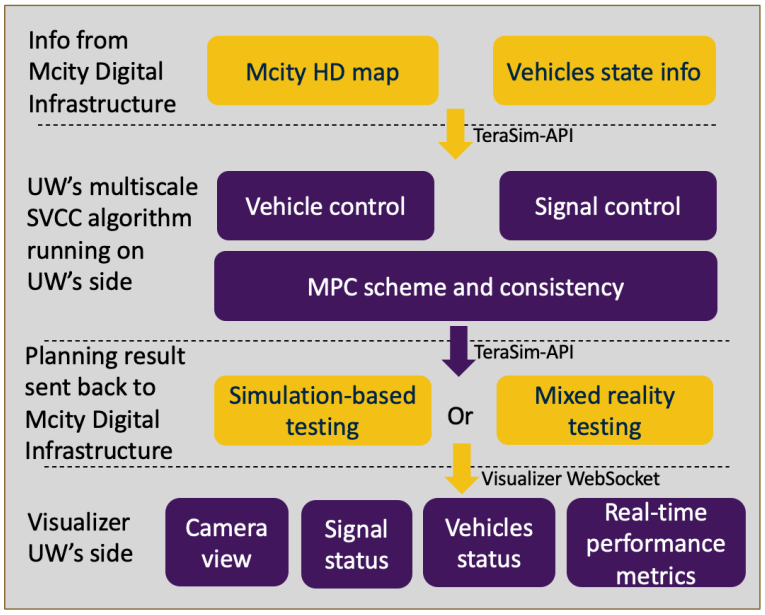

Figure 23. Overview of the testing process

5.3. Test environment

SVCC was tested on an Mcity intersection highlighted in Figure 24. This intersection features four legs and a total of nine incoming lanes, with four primary non-conflicting signal phases depicted in Figure 25. Originally, the intersection operated on a fixed-time scenario with green phases of 15, 30, 30, and 26 seconds, respectively, for phase #1 – phase #4. SVCC, however, allows for dynamic green times, adjustable from a minimum of five seconds to a proper duration the algorithm deems necessary.

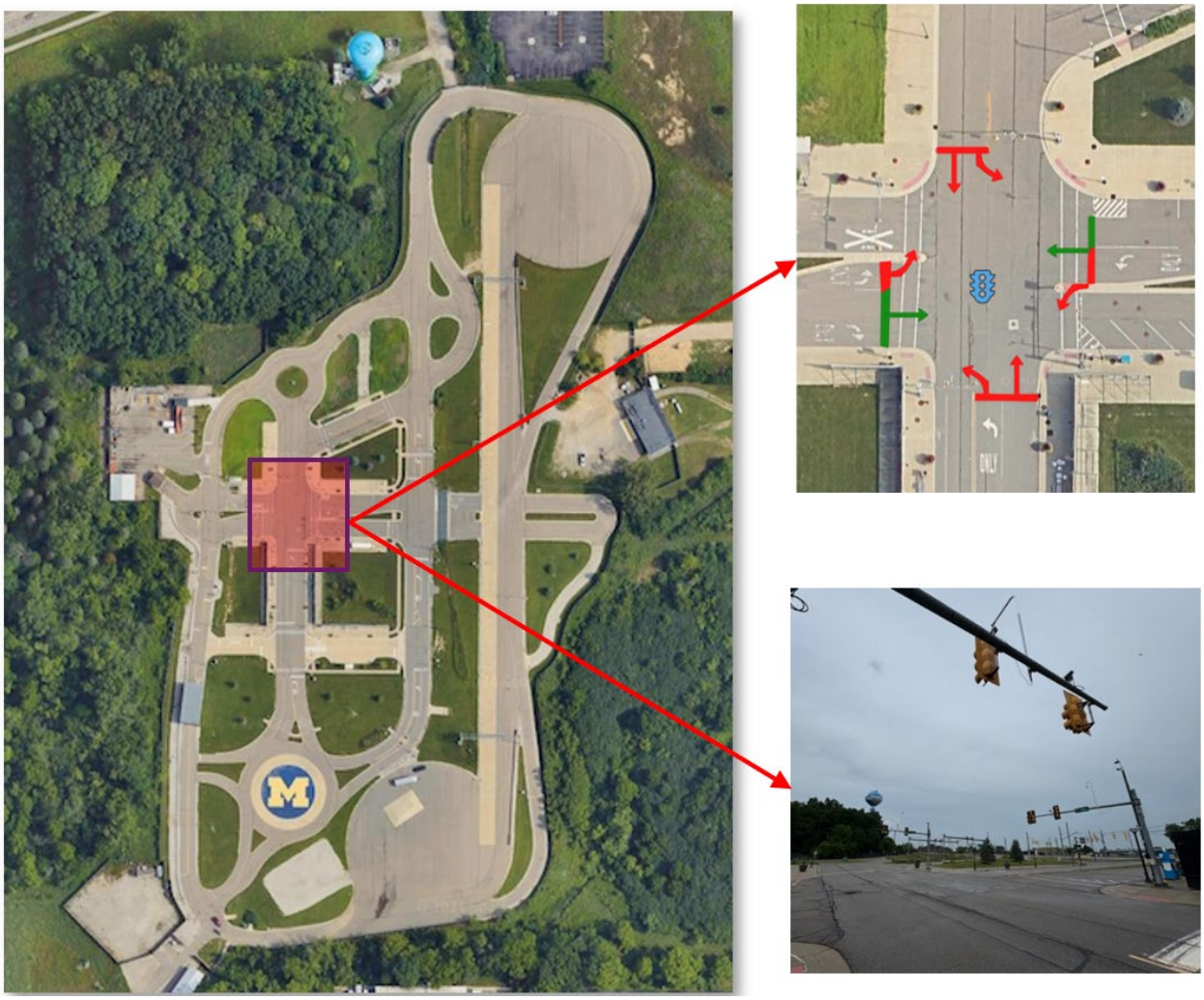

Figure 24. Studied intersection located at Mcity

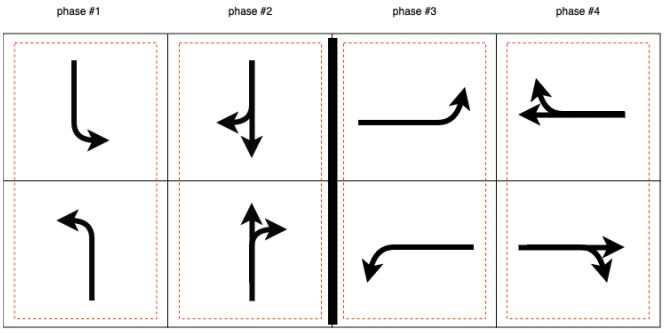

Figure 25. Dual-ring diagram of the signal phases at the studied intersection

SVCC testing was conducted in two environments:

1- Simulation testing: The simulation can run both locally and remotely based on the predefined vehicles, their routes, and the corresponding SUMO XML files. This environment allows for detailed and controlled testing of SVCC and provides an opportunity to evaluate the algorithm's performance under a variety of simulated traffic conditions and scenarios. It also ensures that the algorithm's functionality could be thoroughly examined before the mixed-reality field testing.

2- Mixed-reality remote field testing: This setting combines the real-world and simulated environment to create an augmented mixed-reality testing environment. In this setup, one CAV is physically present in the field, while background vehicles are created in simulation and synchronized with the real-world vehicle using TeraSim. Figure 26 shows the mixed environment, where the red object represents the CAV in the field, and the blue objects represent background vehicles that are synchronized with the field environment through simulation. This approach allows for an assessment of SVCC's performance in real-world traffic conditions and vehicles.

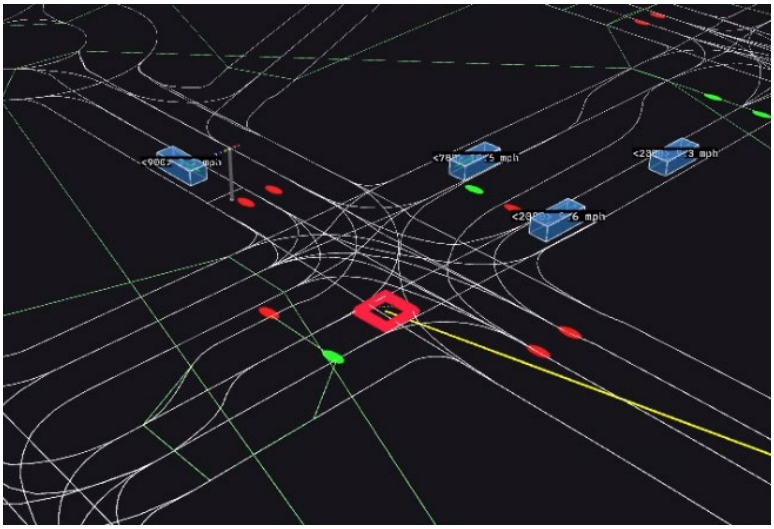

Figure 26. Mixed-reality testing

The configuration parameters and scenario design for the field test were carefully selected to align with the specific characteristics of the test environment and the goals of SVCC. The parameters used are outlined in Table 5.

SVCC was tested under various mixed-flow scenarios to evaluate its performance in different traffic conditions. These scenarios include 100, 75, 50, and 25% penetration rate scenarios. The mixed-reality environment is used to test full penetration (100%), providing a real-world testbed for SVCC, while other penetration rates are evaluated through the simulation platform. This comprehensive approach ensures that the SVCC algorithm's performance is thoroughly assessed across a range of realistic traffic scenarios.

Table 5. Configuration parameters for SVCC testing at Mcity

Parameter	Value
Slower problem scale (ΔT_s)	$5s$
Faster problem scale (ΔT_f)	$0.5s$
Prediction horizon steps (T^s)	6
Number of critical points (h)	3
Car-following headway (τ_h)	$1s$
Car-following safety distance (d_0)	$6.5m$
Maximum acceleration (a_{max})	$4m/s^2$
Minimum acceleration (a_{min})	$-2m/s^2$
Maximum Speed (v_{max})	$5m/s$
Minimum speed (v_{min})	$0m/s$

Signal yellow time	$3s$
Signal all-red time	$1s$

5.4. Required Adjustments

Changes and updates were made to both TeraSim and physical traffic signal infrastructure to be able to conform with the commands given from the remote researcher (i.e., SVCC). TeraSim simulation platform underwent several upgrades to accommodate the real-time interaction with SVCC. The communication speed was significantly increased to minimize latency. Additionally, TeraSim was updated to facilitate the transmission of vehicle control commands and traffic signal control from SVCC directly to the infrastructures. Moreover, the existing physical traffic signals at the Mcity test facility were traditionally set to fixed-time operation, which limited their adaptability to dynamic control commands. To align with the SVCC algorithm's requirements, the traffic signal system was upgraded to enable more flexible and responsive operation in accordance with the SVCC commands.

SVCC also required upgrades due to several challenges. For example, the configuration parameters used in the original SVCC method needed adjustments to align with Mcity's infrastructure, including adjustments according to practical signal timing considerations and the speed/acceleration limits of the real CAVs in the field. Additionally, the communication range at Mcity's intersections was considerably shorter than that in the simulation environment where SVCC was initially tested. Computational efficiency was another major challenge. Real-time control necessitates significant reductions in computational time, requiring updates to both SVCC algorithms and hardware to ensure effective real-time processing. To address these challenges, the following upgrades to SVCC were implemented:

1- Signal Safety Consideration: The time step for the slower-scale problem was set to the minimum green time required by Mcity signals, which is five seconds. This adjustment ensures that signal phase updates do not occur more frequently than this interval, aligning with safety and applicability considerations.
2- Practical Acceleration and Speed of CAVs: The maximum and minimum acceleration ranges for CAVs in Mcity are lower compared to the case study where the SVCC algorithm was originally tested. Consequently, the acceleration range was adjusted from [-5, 4] to [-2, 4] m/s2. Similarly, the maximum speed was reduced from 11 to 5 m/s to match the constraints of the Mcity test environment.
3- Communication Range: This was reduced from 200m to 20m due to the shorter approaching lanes of the test intersection in Mcity. Although this length is much shorter than those of the previously studied intersections, SVCC algorithm was able to perform predictions effectively without any issues. This demonstrates SVCC's flexibility and reliability across different settings.

4- Real-time Execution Requirements: Given the need for real-time control and implementation, SVCC needs to operate within a short time frame. The TeraSim simulator step was set at 0.1 seconds (100 milliseconds), necessitating that SVCC algorithms complete their computations within this duration. To achieve this goal, several changes were made to the GAMS configuration and licensing. Specifically, the slower-scale problem (a MINLP problem) was solved using the SCIP package in GAMS with a relative gap of 0.001, focusing on solution feasibility. For the faster-scale problem, which is a Nonlinear Programming (NLP) problem, the CONOPT package was used, significantly improving running speed compared to the previously used IPOPT package. Overall, these updates ensure that the solving time of SVCC algorithms (both the slower-scale problem and the faster-scale problem) is within 100 milliseconds for most of the times.

5.5. Results

The performance of SVCC was assessed using output files from the SUMO simulation, including data on emissions, queues, and trip information, along with outputs from the surrogate safety measures (SSM) device, which provide information on conflicts between the ego vehicle and other vehicles using metrics such as TTC, Distance to Risk Assessment Collision (DRAC), Potential Emergency Time (PET), etc. For further details, one may refer to the SUMO documentation (SUMO, 2024). The number of conflicts presented in Figure 27 is the count of instances where the TTC is less than three seconds. TTC is determined by dividing the distance between two vehicles by the speed difference, considering only cases where the following vehicle is traveling faster than the leading vehicle.

As mentioned earlier, the 100% CAV penetration scenario was evaluated in the mixed reality field test setting. In this setup, real-world data from the Mcity testing facility was integrated with simulated data to create a comprehensive testing environment. The output results from the mixed-reality field testing were transmitted directly to the remote researchers for performance metrics calculation. As illustrated in Figure 27, it is evident that in the 100% penetration case, the average fuel consumption, waiting time, time loss, and queue length performance metrics are much improved under the SVCC scenario compared to the conditions where the traffic signal at the intersection is controlled under the fixed-time or actuated modes. The number of vehicles passing the intersection is almost the same under the three types of control.

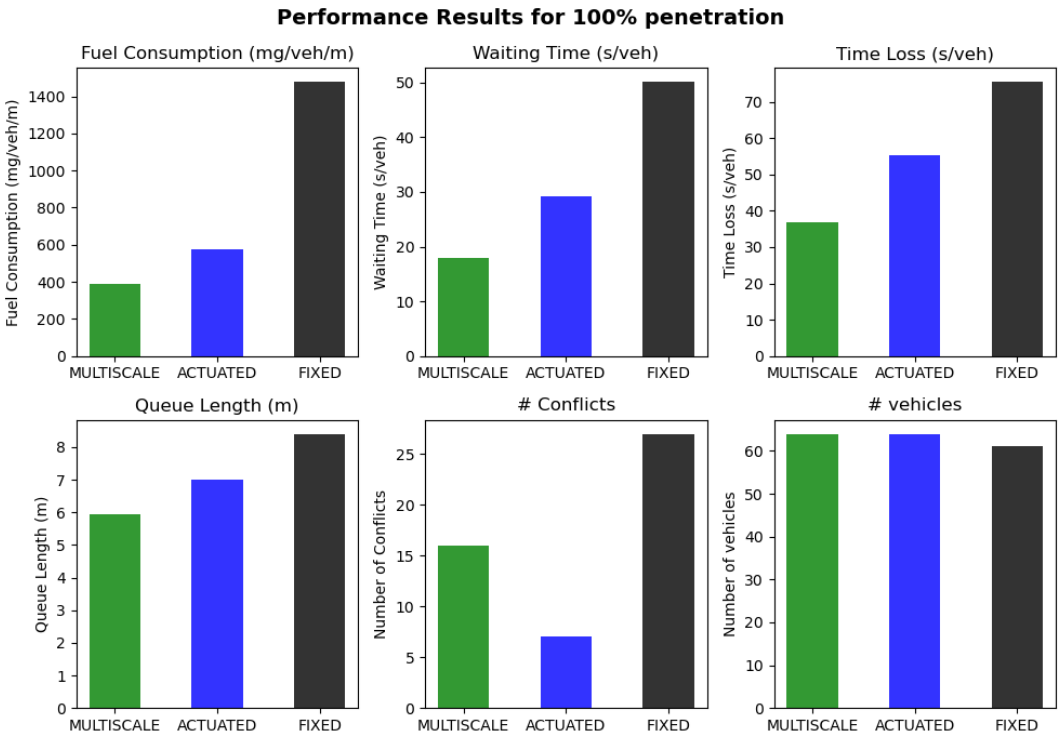

Figure 27. Performance result of 100% penetration (comparison between fixed, actuated, and multiscale SVCC scenarios)

Regarding the higher number of conflicts observed in the SVCC control compared to the actuated control, it is important to note that the conflicts considered here are limited to lead/follow conflicts. This is because the intersection under study does not involve merging, crossing, or diverging conflicts thanks to the signal timing design (see Figure 25) and the specific geometry of the intersection (see Figure 24). As the SVCC method tries to utilize green time more efficiently, it naturally leads to slightly shorter time headways, resulting in more TTCs. More importantly, the TTC threshold used in this study is set at three seconds. In many studies involving CAVs, a more stringent TTC limit of 1.5 seconds is often used (Rahman et al., 2019). If a TTC limit of 1.5 seconds were applied in this study, the number of conflicts across all scenarios would be zero, as all measured conflicts fall within the two to three second range.

The mixed-flow cases (with both CAVs and HDVs) were tested in simulation. Figure 28 illustrates the results for the abovementioned metrics across different penetration rate scenarios. As shown, almost all performance metrics (except for the number of conflicts which shows mixed results) are improved under the SVCC scenario compared with the fixed-time and actuated settings. Additionally, the performance of SVCC improves with increasing penetration rates. These results highlight the overall effectiveness SVCC control in enhancing traffic management and operational efficiency as more CAVs are introduced into the system. As aforementioned, while the comparisons and performance

evaluations are done in the simulation environment for the 75%, 50%, and 25% scenarios, very similar results are expected when the experiments (under different penetrations) are conducted in the mixed reality field testing since CAVs and the hardware (signals) are controlled under exactly the same algorithms. The only factor that may bring discrepancy between the simulation results and the field testing results is the impacts of the background HDVs when the CAV penetration rate is not 100%. The driving behaviors of HDVs and/or how they interact with CAVs may be different in simulation and in the real-world situations, which may result in difference experimental performances. Here we assume such difference is marginal; see the next section for more discussions regarding this aspect.

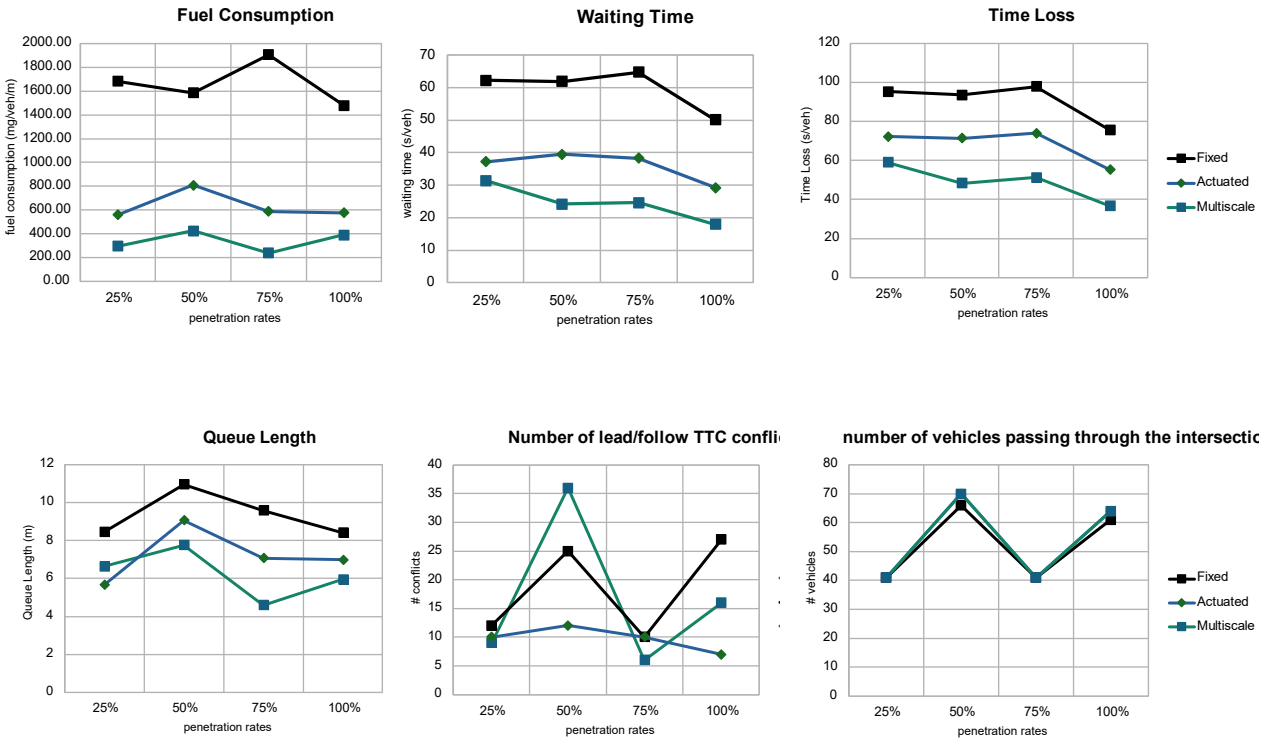

Figure 28. Performance results for different penetration rates (25%, 50%, 75%, and 100%)

6. Conclusion and Future Direction

This project developed a multiscale, multimodal SVCC (M^2SVCC) algorithm by integrating active transportation users (pedestrians and cyclists) and vehicles of different types. Initial results demonstrated significant improvements in pedestrian time loss, vehicle waiting time, vehicle time loss, queue length, as well as power consumption and fuel consumption for different vehicle types (i.e., ICE and EVs). Performance gains were observed in both concurrent and exclusive pedestrian phasing settings, with the exclusive phase offering greater safety (fewer conflicts) and increased flexibility in performance control. Additionally, the algorithm optimized interactions among vehicles, pedestrians, and cyclists, enhancing the overall multimodal performances.

The research also investigated deploying and evaluating the multiscale SVCC algorithm (Guo & Ban, 2023) on a signalized intersection at Mcity. Utilizing Mcity 2.0's remote access platform, the SVCC algorithm was tested across different penetration rate scenarios and in both simulation and mixed-reality environments. The findings demonstrated that the multiscale SVCC algorithm offers significant advantages over traditional fixed-time and actuated signal timing control methods in both simulation and real-world settings.

The future direction of this research includes the following:

1- Applying learning methods that are most effective for managing multimodal signalized intersections with CAVs: While this study employed a model-based approach, future research should investigate learning techniques to enhance signalized intersection control in the multiscale, multimodal environments. Potential methods include Imitation Learning, knowledge distillation, and Deep Reinforcement Learning to dynamically optimize signal timing and CAV control based on real-time traffic conditions.
2- More numerical results and discussions to illustrate the performance of the proposed M^2SVCC framework: This will include **analysis** on the performance of the M^2SVCC on bigger networks with multiple signalized intersections.
3- Implement and test M^2SVCC (with pedestrians and bicyclists) in the Mcity 2.0 testbed: Building on the initial evaluation at Mcity, future work should focus on **multimodal deployment and testing** of the M2SVCC framework, including pedestrian and cyclist integration on multiple intersections in Mcity.

References

AV Crashes. (2024). https://www.avcrashes.net/?id=768&type=autonomous

Ban, X. (Jeff), Yang, D., Wang, J., & Hamdar, S. (2020). Editorial: Connected and automated vehicles (CAV) based traffic-vehicle control. *Transportation Research Part C: Emerging Technologies*, *112*, 116–119. https://doi.org/10.1016/j.trc.2020.01.011

Brand, C., Dons, E., Anaya-Boig, E., Avila-Palencia, I., Clark, A., de Nazelle, A., Gascon, M., Gaupp-Berghausen, M., Gerike, R., Götschi, T., Iacorossi, F., Kahlmeier, S., Laeremans, M., Nieuwenhuijsen, M. J., Pablo Orjuela, J., Racioppi, F., Raser, E., Rojas-Rueda, D., Standaert, A., … Int Panis, L. (2021). The climate change mitigation effects of daily active travel in cities. *Transportation Research Part D: Transport and Environment*, *93*, 102764. https://doi.org/10.1016/j.trd.2021.102764

Fayazi, S. A., & Vahidi, A. (2018). Mixed-Integer Linear Programming for Optimal Scheduling of Autonomous Vehicle Intersection Crossing. *IEEE Transactions on Intelligent Vehicles*, *3*(3), 287–299. IEEE Transactions on Intelligent Vehicles. https://doi.org/10.1109/TIV.2018.2843163

Fayazi, S. A., Vahidi, A., & Luckow, A. (2019). A Vehicle-in-the-Loop (VIL) verification of an all-autonomous intersection control scheme. *Transportation Research Part C: Emerging Technologies*, *107*, 193–210. https://doi.org/10.1016/j.trc.2019.07.027

Feng, Y., & Liu, H. (2019). *Development of an Augmented Reality Environment for Connected and Automated Vehicle Testing*. SDOT CCAT Project No. 2. http://hdl.handle.net/2027.42/149453

Feng, Y., Yu, C., Xu, S., Liu, H. X., & Peng, H. (2018). An Augmented Reality Environment for Connected and Automated Vehicle Testing and Evaluation. *2018 IEEE Intelligent Vehicles Symposium (IV)*, 1549–1554. https://doi.org/10.1109/IVS.2018.8500545

FHWA. (2021). *Traffic Signal Timing Manual: Chapter 5—Office of Operations*. https://ops.fhwa.dot.gov/publications/fhwahop08024/chapter5.htm

Fiori, C., Ahn, K., & Rakha, H. A. (2016). Power-based electric vehicle energy consumption model: Model development and validation. *Applied Energy*, *168*, 257–268. https://doi.org/10.1016/j.apenergy.2016.01.097

Guo, Q. (2022). *Multi-Scale Signal-Vehicle Coupled Control with Connected and Autonomous Vehicles* [Doctoral Dissertation]. University of Washington.

Guo, Q., & Ban, X. (Jeff). (2023). A multi-scale control framework for urban traffic control with connected and automated vehicles. *Transportation Research Part B: Methodological*, *175*, 102787. https://doi.org/10.1016/j.trb.2023.102787

Guo, Q., & Ban, X. (Jeff). (2024). Network multiscale urban traffic control with mixed traffic flow. *Transportation Research Part B: Methodological*, *185*, 102963. https://doi.org/10.1016/j.trb.2024.102963

Guo, Q., Li, L., & (Jeff) Ban, X. (2019). Urban traffic signal control with connected and automated vehicles: A survey. *Transportation Research Part C: Emerging Technologies*, *101*, 313–334. https://doi.org/10.1016/j.trc.2019.01.026

Han, X., Ma, R., & Zhang, H. M. (2020). Energy-aware trajectory optimization of CAV platoons through a signalized intersection. *Transportation Research Part C: Emerging Technologies*, *118*, 102652. https://doi.org/10.1016/j.trc.2020.102652

IEA. (2024). *Trends in electric cars – Global EV Outlook 2024*. International Energy Agency. https://www.iea.org/reports/global-ev-outlook-2024/trends-in-electric-cars

Jiang, H., Yao, Z., Zhang, Y., Jiang, Y., & He, Z. (2024). Pedestrian shuttle service optimization for autonomous intersection management. *Transportation Research Part C: Emerging Technologies*, *163*, 104623. https://doi.org/10.1016/j.trc.2024.104623

Khalighi, F., & Christofa, E. (2015). Emission-Based Signal Timing Optimization for Isolated Intersections. *Transportation Research Record*, *2487*(1), 1–14. https://doi.org/10.3141/2487-01

Lee, H., Kang, M., Hwang, K., & Yoon, Y. (2024). The typical AV accident scenarios in the urban area obtained by clustering and association rule mining of real-world accident reports. *Heliyon*, *10*(3), e25000. https://doi.org/10.1016/j.heliyon.2024.e25000

Liu, H. (2023). *Safety Assessment for Highly Automated Vehicles*. https://static1.squarespace.com/static/526c7a98e4b023d8f09390ed/t/657caeb2f521406e97a7e445/1702670003959/liu+dec+2023+slides.pdf

Ma, J., Zhou, F., Huang, Z., & James, R. (2018b). Hardware-In-The-Loop Testing of Connected and Automated Vehicle Applications: A Use Case For Cooperative Adaptive Cruise Control. *2018 21st International Conference on Intelligent Transportation Systems (ITSC)*, 2878–2883. https://doi.org/10.1109/ITSC.2018.8569753

Ma, J., Zhou, F., Huang, Z., Melson, C. L., James, R., & Zhang, X. (2018). Hardware-in-the-Loop Testing of Connected and Automated Vehicle Applications: A Use Case for Queue-Aware Signalized Intersection Approach and Departure. *Transportation Research Record*, *2672*(22), 36–46. https://doi.org/10.1177/0361198118793001

McConky, K., & Rungta, V. (2019). Don't pass the automated vehicles!: System level impacts of multi-vehicle CAV control strategies. *Transportation Research Part C: Emerging Technologies*, *100*, 289–305. https://doi.org/10.1016/j.trc.2019.01.024

Mcity Website. (2024). *Mcity test facility*. Mcity Test Facility. https://mcity.umich.edu/what-we-do/mcity-test-facility/

Mueller, N., Rojas-Rueda, D., Cole-Hunter, T., de Nazelle, A., Dons, E., Gerike, R., Götschi, T., Int Panis, L., Kahlmeier, S., & Nieuwenhuijsen, M. (2015). Health impact assessment of active transportation: A systematic review. *Preventive Medicine*, *76*, 103–114. https://doi.org/10.1016/j.ypmed.2015.04.010

Niels, T., Bogenberger, K., Mitrovic, N., & Stevanovic, A. (2020). Integrated Intersection Management for Connected, Automated Vehicles, and Bicyclists. *2020 IEEE 23rd International Conference on Intelligent Transportation Systems (ITSC)*, 1–8. https://doi.org/10.1109/ITSC45102.2020.9294600

Niels, T., Bogenberger, K., Papageorgiou, M., & Papamichail, I. (2024). Optimization-Based Intersection Control for Connected Automated Vehicles and Pedestrians. *Transportation Research Record*, *2678*(2), 135–152. https://doi.org/10.1177/03611981231172956

Niels, T., Mitrovic, N., Dobrota, N., Bogenberger, K., Stevanovic, A., & Bertini, R. (2020). Simulation-Based Evaluation of a New Integrated Intersection Control Scheme for Connected Automated Vehicles and Pedestrians. *Transportation Research Record*, *2674*(11), 779–793. https://doi.org/10.1177/0361198120949531

Osorio, C., & Nanduri, K. (2015). Urban transportation emissions mitigation: Coupling high-resolution vehicular emissions and traffic models for traffic signal optimization. *Transportation Research Part B: Methodological*, *81*, 520–538. https://doi.org/10.1016/j.trb.2014.12.007

Piperigkos, N., Lalos, A. S., & Berberidis, K. (2022). Alternating optimization for multimodal collaborating odometry estimation in CAVs. *2022 30th Mediterranean Conference on Control and Automation (MED)*, 670–675. https://doi.org/10.1109/MED54222.2022.9837156

Pourmehrab, M., Emami, P., Martin-Gasulla, M., Wilson, J., Elefteriadou, L., & Ranka, S. (2020). Signalized Intersection Performance with Automated and Conventional Vehicles: A Comparative Study. *Journal of Transportation Engineering, Part A: Systems*, *146*(9), 04020089. https://doi.org/10.1061/JTEPBS.0000409

Rabl, A., & de Nazelle, A. (2012). Benefits of shift from car to active transport. *Transport Policy*, *19*(1), 121–131. https://doi.org/10.1016/j.tranpol.2011.09.008

Rahman, M. S., Abdel-Aty, M., Lee, J., & Rahman, M. H. (2019). Safety benefits of arterials' crash risk under connected and automated vehicles. *Transportation Research Part C: Emerging Technologies*, *100*, 354–371. https://doi.org/10.1016/j.trc.2019.01.029

Sallis, J. F., Frank, L. D., Saelens, B. E., & Kraft, M. K. (2004). Active transportation and physical activity: Opportunities for collaboration on transportation and public health research. *Transportation Research Part A: Policy and Practice*, *38*(4), 249–268. https://doi.org/10.1016/j.tra.2003.11.003

Shladover, S. E. (2018). Connected and automated vehicle systems: Introduction and overview. *Journal of Intelligent Transportation Systems*, *22*(3), 190–200. https://doi.org/10.1080/15472450.2017.1336053

SUMO. (2024). *Output—SUMO Documentation*. https://sumo.dlr.de/docs/Simulation/Output/index.html

Sun, C., Guanetti, J., Borrelli, F., & Moura, S. J. (2020). Optimal Eco-Driving Control of Connected and Autonomous Vehicles Through Signalized Intersections. *IEEE Internet of Things Journal*, *7*(5), 3759–3773. IEEE Internet of Things Journal. https://doi.org/10.1109/JIOT.2020.2968120

Vellamattathil Baby, T., Karimi Shahri, P., Ghasemi, A. H., & HomChaudhuri, B. (2021, January 18). *Suggestion-Based Fuel Efficient Control of Connected and Automated Vehicles*. ASME 2020 Dynamic Systems and Control Conference. https://doi.org/10.1115/DSCC2020-3193

Wu, W., Liu, Y., Hao, W., Giannopoulos, G. A., & Byon, Y.-J. (2022). Autonomous intersection management with pedestrians crossing. *Transportation Research Part C: Emerging Technologies*, *135*, 103521. https://doi.org/10.1016/j.trc.2021.103521

Wu, X., Freese, D., Cabrera, A., & Kitch, W. A. (2015). Electric vehicles' energy consumption measurement and estimation. *Transportation Research Part D: Transport and Environment*, *34*, 52–67. https://doi.org/10.1016/j.trd.2014.10.007

Yao, H., & Li, X. (2020). Decentralized control of connected automated vehicle trajectories in mixed traffic at an isolated signalized intersection. *Transportation Research Part C: Emerging Technologies*, *121*, 102846. https://doi.org/10.1016/j.trc.2020.102846

Yu, C., Feng, Y., Liu, H. X., Ma, W., & Yang, X. (2018). Integrated optimization of traffic signals and vehicle trajectories at isolated urban intersections. *Transportation Research Part B: Methodological*, *112*, 89–112. https://doi.org/10.1016/j.trb.2018.04.007

Zhao, Y., & Zhang, H. M. (2017). A unified follow-the-leader model for vehicle, bicycle and pedestrian traffic. *Transportation Research Part B: Methodological*, *105*, 315–327. https://doi.org/10.1016/j.trb.2017.09.004

Appendix: Notations

Symbol	Definition	Unit
α	Vehicle weighting factor	-
β	Pedestrian weighting factor	-
γ	Bicycle weighting factor	-
k_s	Slower scale time step	-
k_f	Faster scale time step	-
h	Critical time steps	-
$a_{i,j}(k_s)$	Acceleration of vehicle i on lane j at time step k_s	m/s^2
$v_{i,j}(k_s)$	Speed of vehicle i on lane j at time step k_s	m/s
$s_{i,j}(k_s)$	Position of vehicle i on lane j at time step k_s	m
$f_{i,j}(k_s)$	Fuel rate of vehicle i on lane j at time step k_s	mg/s
$g_{i,j}(k_s)$	Whether vehicle i on lane j has crossed the stop-line at time step k_s ($g_{i,j}$= 0)	binary
$\tilde{g}_{i,j}(k_s)$	Whether vehicle i on lane j has crossed the safety distance at time step k_s ($\tilde{g}_{i,j}$= 1) (refer to Guo & Ban (2023)).	binary
$p_l(k_s)$	Whether the phase l at time step k_s is on ($p_l = 1$)	binary
$r_j(k_s)$	Whether the lane j at time step k_s has the right of way ($r_j = 1$)	binary
τ_h	Time headway	s
d_0	Safety distance	m
$\Delta T_s, \Delta T_f$	Step length of the slower, and faster scale problems respectively	s
$q_m(k_s)$	Whether crossing m at time step k_s has the right of way ($q_m = 0$) or not ($q_m = 1$)	binary
$D_m(k_s)$	Pedestrian Demand on crossing m at time step k_s	-
G_p	Pedestrian minimum green time	s
L	Crossing length	m
S_p	Average pedestrian speed (~ 1)	m/s
N_p	number of pedestrians crossing at the corresponding phase and during the slower time slot	-
W	Crossing width	m
$q_n(k_s)$	Whether bike lane n at time step k_s has the right of way ($q_n = 0$) or not ($q_n = 1$)	binary
$D_n(k_s)$	Bicycle Demand on bike lane n at time step k_s	-
A^{J*L}	Mapping function from signal phase to right of way of vehicle lanes	-
B^{M*L}	Mapping function from signal phase to right of way of pedestrian crossings	-
C^{N*L}	Mapping function from signal phase to right of way of bike lanes	-
m_i	Mass of object i	kg
v_i	Speed of object i	m/s
v_i^0	Desired speed of object i	m/s
τ	Relaxation time period	s

d	Distance from the leading object	m
k	Constant of proportionality (refer to Zhao & Zhang (2017))	$1/s$
A_i, B_i	Constants used in repulsive force equations	
d_{ij}	Center distance between objects i and j	m
r_{ij}	Sum of the objects i and j radii	m
n_{ij}	Normalized vector from object i to j	
d_{iw}	Distance of objects i from boundary w	m
n_{iw}	Normalized vector perpendicular to the boundary w	